12-1-2011

Spatiotemporal dynamics of transport in the squid giant axon : competition between cargo motor receptors, JIP-1, APP-C, and negative charge

Pamela Seamster

Pamela E Seamster

Candidate

BIOMEDICAL SCIENCES GRADUATE PROGRAM

Department

This thesis is approved, and it is acceptable in quality
and form for publication:

Approved by the Thesis Committee:

Elaine L Bearer, MD PhD , Chairperson

Steven Koch, PhD

Diane Lidke, PhD

Bill Shuttleworth, PhD

Stan Steinberg, PhD

**Spatiotemporal Dynamics of Transport in the Squid Giant Axon:
Competition between cargo motor receptors, JIP-1, APP-C and negative charge**

BY

Pamela E Seamster

BACHELOR OF SCIENCE, BIOLOGY 2004

MASTER OF SCIENCE, BIOMEDICAL SCIENCES, 2011

THESIS

Submitted in Partial Fulfillment of the
Requirements for the Degree of

Master of Science

Biomedical Sciences

The University of New Mexico
Albuquerque, New Mexico

December 2011

DEDICATION

       I wish to dedicate this to my wonderful husband and family for their continued love, support, and encouragement.

ACKNOWLEDGEMENTS

SPATIOTEMPORAL DYNAMICS OF TRANSPORT IN THE SQUID GIANT AXON: COMPETITION BETWEEN CARGO MOTOR RECEPTORS, JIP-1, APP-C, AND NEGATIVE CHARGE

by

Pamela E Seamster

B.S., Biology, The University of Texas at Austin, 2004

M.S., Biomedical Sciences, University of New Mexico, 2011

ABSTRACT

Transport of membrane-bound organelles is critical to neuronal cell function yet mechanisms hitching vesicles to transport machinery remain elusive. Here we test whether jun-kinase interacting protein (JIP-1), a peripheral membrane scaffolding protein that binds kinesin light chain, is sufficient to mediate cargo transport in axons and study its competition with amyloid precursor protein cytoplasmic domain (APP-C) and negative charge, also known motor receptors. Fluorescent beads (100 nm diameter) exhibit sequence-specific fast anterograde transport (0.46μm/s instantaneous velocity) in the squid giant axon when conjugated to a 14-amino acid synthetic peptide derived from the carboxyl terminus of JIP-1. JIP-1-beads have statistically significant faster velocities, longer run lengths, and fewer pauses of shorter durations than APP-C or negatively charged beads by cumulative

probability analyses of thousands of motile beads compared by a nonparametric K-S test, with a P=0.004. In competition experiments negatively charged beads gradually cease moving when co-injected with either APP-C or JIP-1 beads, which sustain 90% motility. Co-injection of APP-C and JIP-1 beads decreases each bead's propensity to move initially. At later time points JIP-1-beads recover frequency without further decreasing APP-C moves, suggesting JIP-1 recruits motors from a cryptic pool not accessible to APP-C. Soluble JIP-1 peptide inhibits JIP-1 beads, with smaller effects on APP-C and negatively charged beads. Thus the hierarchy for recruitment of transport machinery is JIP>APP>negative charge. Organelle transport may in part be regulated through the numbers, types and affinities of motor receptors displayed on each organelle's cytoplasmic surface.

TABLE OF CONTENTS

Chapter 1: Introduction and Specific Aims

Intracellular transport is a complex dynamic process that requires intricate coordination of multiple components in order to develop and maintain viability of a cell. Vesicular transport carries organelles to and from the cell surface. Incoming particles carry signals from the plasma membrane and from the extracellular environment and are thus important for the cell's ability to respond to external cues or pathogens. Outgoing transport typically passes through the Golgi apparatus and carries molecules destined for the plasma membrane or for secretion. Some intracellular transport involves organelles that do not enter or leave the cell, such a mitochondria, whose function may be needed in different areas of the cell at different moments in its life cycle (Hirokawa and Takemura, 2004).

The components of transport are the tracks, composed of actin and/or microtubule polymers, the cargo that is being transported, including packets of RNA, proteins, vesicular cargo, and subunits of the tracks themselves, and finally, the molecular motors, consisting of the myosin family, the kinesin family, and dynein, that facilitate cargo transport. While there is a depth of knowledge regarding the tracks and the motors, one major gap in the field of transport is the understanding of how cargo attaches to motors for transport (Kamal and Goldstein, 2002 and Karcher, et al, 2002). Another gap regards how cargo transport is regulated. Regulation probably involves modifications of each of the three components, the tracks, the cargo and/or the motors (Morfini, et al, 2009).

One cell type that is particularly dependent on efficient transport is the neuron. Neurons are highly polarized, consisting of a cell body, dendrites, and a long axon extending out to the cell synapse. The axon extends far from the cell body out to the synapse; in humans they can be up to a meter or more in length. The length of these axons requires efficient and coordinated transport in order to deliver cargo out to the synapse (anterograde transport) and back to the nucleus (retrograde transport) in the cell body. An ideal cellular model for studying this transport is the giant axon of the squid, *Loligo pealei.* After the Hodgkin and Huxley work in squid axons received the Nobel Prize for discovery of the electrical basis of neuronal signaling, the squid giant axon became a popular physiological tool for other major discoveries in neuronal mechanisms (Hodgkin, et al, 1952a, and Hodgkin and Huxley, 1952b, 1952c, and 1952d). These so-called giant axons are up to 7cm in length and 0.8mm wide and when dissected from the squid they maintain viability for hours.

Original studies of transport mechanisms were based on injection of radiolabeled compounds into the eye and measurements of their progress at various time points afterwards in autoradiograms (Forman, et al, 1971, Grafstein and Laureno, 1973, and most recently, Yuan, et al, 2008). Since transport from the retina into the optic nerve is exclusively anterograde, these studies did not address any aspect of retrograde transport. These radiogram-based measurements did identify two types of transport: fast and slow (McEwen and Grafstein, 1968). Slow transport was sub-divided into two components, slow compartment A and B, with different proteins in each and different rates of progress along the optic nerve. The components that moved by fast axonal transport were identified as being primarily membrane proteins, or proteins expected to be within

secretory-type granules derived from the Golgi apparatus (McEwen et al, 1971, Elluru, et al, 1995, and Yuan, et al, 2008). However, these studies do not provide any insight into the mechanisms of how cargo is transported, or how cargo transport is regulated.

Negatively charged particles were shown to transport in crab axons (Adams and Bray, 1982) and subsequent studies began to exploit the squid giant axon to define the mechanisms that regulate cargo transport. Squid axoplasm can be extruded from the axon sheath (Brady and Lasek, 1982a) and video enhanced contrast differential interference microscopy led to the characterization of fast axonal transport of membranous organelles that transport both anterograde and retrograde in extruded axoplasm (Brady, et al, 1982b). Further use of extruded axoplasm allowed for the isolation and characterization of movements of organelles along single filament tracks (Schnapp, et al, 1985, and Vale, et al, 1985b). Due to the uniformly oriented microtubules of axons, with the plus-ends (transport toward is anterograde) pointed toward the synaptic terminal and the minus ends (transport toward is retrograde) pointed toward the nucleus (Heidemann, et al, 1981), subsequent experiments were able to identify different axoplasmic proteins that were responsible for anterograde and retrograde transport (Vale, et al, 1985d). An observation that ATP was required for this transport led to studies using non-hydrolysable AMP-PNP (Lasek and Brady, 1985), which led to the discovery of kinesin-1 (also known as conventional kinesin) as the motor associated with fast axonal anterograde transport along microtubule tracks (instantaneous velocities of 0.1-0.5 microns/sec) (Vale, et al, 1985a, and Lasek and Brady, 1985). Shortly after the discovery of kinesin-1 as an anterograde motor, the Vallee lab discovered that one of the high molecular weight microtubule-binding proteins, MAP 1C,

was also an ATPase and mediated transport in the retrograde direction (Paschal, et al, 1987a, and Paschal and Vallee, 1987b). This was later characterized as the molecular motor dynein (Schnapp and Reese, 1989, and Schroer, et al, 1989).

Subsequent studies revealed that dynein (MAP1C) might require a host of other proteins to connect with cargo, including a UV-sensitive adaptor, Dynactin (Schroer and Sheetz, 1991, and Gill, et al, 1991). The ability to separate anterograde and retrograde moving organelles from squid axoplasm allowed further detail of these different motors activities, anterograde and retrograde, to be studied (Schnapp, et al, 1992, and Muresan, et al, 1996).

After the identification of kinesin-1 as the motor for fast axonal anterograde transport of vesicular cargo, there was still a gap in knowledge of how other cellular components, such as cytoskeletal elements and neurofilaments, that compose the slow transport compartment, are transported. Fast axonal transport of vesicles was shown to occur at maximum rates of 1-5 microns/second (Allen, et al, 1982 and Brady, et al, 1982b), while transport of cytoskeletal elements occurred at rates of 0.2-4mm/day (Lasek, 1986). These two different rates are described as fast and slow axonal transport, respectively.

In order to better understand the mechanisms of slow axonal transport, fluorescent cytoskeletal elements were injected into the giant axon of the squid and observed for transport (Terasaki, et al, 1995). In this study, all negatively charged particles smaller than 500nm, including microtubules and actin filaments were observed to displayed similar maximum velocities, consistent with transport by kinesin-1, in the anterograde

4

direction. However, smaller particles paused less frequently, and thus traveled a farther distance over the same amount of time. This led to the conclusion that fast and slow axonal transport may be carried out by the same motor, kinesin-1, but elements transported at the slow axonal transport rate display more pauses for longer durations. Recent work has confirmed this in other systems (Jung and Brown, 2009, Prahlad, et al, 2000, and Chou, et al, 2001).

After the discovery of kinesin-1, intensive effort was put forth towards understanding the structure of kinesin-1, and how it moves along microtubules. The structure of kinesin-1 is made up of two kinesin heavy chains (KHCs) (Yang, et al, 1989) encoded by three genes (Kanai, et al, 2000), and two kinesin-1 light chains (KLCs) encoded by three genes (Rahman, et al, 1998). It is these light chains that are proposed to be the sites of membranous and other cargo attachment (Hirokawa, et al, 1989). The kinesin-1 heavy chains each contain an N-terminal motorized head responsible for ATP hydrolysis and binding to microtubules (Yang, et al 1990), a neck linker region, a stalk domain used to dimerize with a second heavy chain, and a C-terminal tail region which interacts with the light chains. The kinesin-1 holoenzyme moves processively along the microtubules, leaving one head attached while the other 'swings' around, the force for such movement generated by tension in the neck region through hydrolysis of ATP (Vale and Fletterick, 1997). Through this 'stepping' mechanism, kinesin-1 takes 8nm steps for each ATP hydrolyzed (Svoboda et al, 1993, Coy, et al 1999, Yildiz, et al, 2004, and Yildiz, et al, 2008).

While kinesin-1 was being characterized, other motors involved in axonal transport were being discovered. Kinesin II was first identified in sea urchin (Cole, et al,

1993). It was later found in other organisms including squid and mammals and has a similar structure to kinesin-1, with the N-terminal region containing the motor domains. Kinesin-3 was first discovered as Unc104 in C. elegans (Hall and Hedgecock, 1991) and has also been found in squid and other mammals. It too has a similar structure to kinesin-1, with the motor domains at the N-terminus of the heavy chains. Kinesin 3 is found in the squid axon and is almost exclusively bound to organelles with little in the soluble compartment (DeGiorgis, et al, 2008). To date, up to as many as 50 kinesins have been identified (Muresan, 2000). However, due to the similarity of their structures, Kinesin-1, kinesin II, and kinesin-3 are believed to be the three main kinesins involved in anterograde axonal transport (Muresan, 2000).

Kinesin-1 has been shown to be associated with membranous organelles (Schnapp, et al, 1992), but has also been shown to exist in a large cytoplasmic pool in squid axoplasm (Brady, et al, 1990). Kinesin II has been also shown to be associated with vesicles isolated from squid and has a small axoplasmic fraction (Muresan, et al, 1998). Finally, kinesin-3 seems to be primarily associated with organelles in the squid (DeGiorgis, et al, 2008). Kinesin-1, as previously described, has been shown to associate with negatively charged particles (Vale, et al, 1985c, and Terasaki, et al, 1995), and Unc104/kinesin-3 has been shown to have a pleckstrin homology domain that interacts with phosphatidylinositol(4,5)bisphosphate residues on the membranes of synaptic vesicles (Klopfenstein, et al, 2002, and Klopfenstein and Vale, 2004).

While extensive effort has been made to understand which of the kinesins are present, how they move, and how they are distributed in the axon (either with or without cargo), little has been done to decipher exactly what membrane properties of cargo (aside

from negative charge and phosphatidylinositol(4,5)bisphosphate residues) allow for binding to these motors for transport, and how this effects the regulation of cargo transport. Due to the abundance of kinesin-1 in the axon and the light chains believed to interact with cargo, the most effort has gone in to understanding what membrane proteins might serve as cargo motor receptors for these kinesin light chains.

One of the first published studies aimed at identifying a protein receptor for kinesin identified kinectin, an integral membrane protein on the endoplasmic reticulum in chick brain microsomes (Toyoshima, et al, 1992). This protein was found to interact with kinesin-1, and became the first known protein motor receptor on membranous organelles (Kumar, et al, 1995). Kinectin was quickly gaining consideration as a 'universal peptide cargo motor receptor', until a genetic screen of the Drosophila genome found no genes with any sequence similarity to kinectin (Golstein and Gunawardena, 2000). The lack of a protein such as kinectin in Drosophila meant it could not be a universal peptide cargo motor receptor for kinesin-1. However, this was the first identification of a peptide cargo motor receptor, and many investigators have since sought to identify other peptide cargo motor receptors through biochemical binding studies and through yeast-two-hybrid screens (Horiuchi, et al, 2005, Kamal, et al, 2000, and Verhey, et al, 2001). While these studies are valuable in identifying putative peptide motor receptors, they cannot conclusively identify a direct role in motor recruitment and transport of cargo through these interactions. Additionally, studies with individual putative cargo motor receptors cannot provide any insight into the regulatory transport mechanisms of multiple motile cargos, or how multiple motile cargos may interact.

Specific Aims

Understanding how a cell selects cargo for and regulates cargo transport will advance significantly the understanding of development, maintenance, and functionality of an axon. The field of axonal transport is lacking currently in its understanding of what characteristics of cargo recruit transport machinery and of the spatiotemporal regulatory mechanisms of fast anterograde transport of cargo.

Amyloid precursor protein (APP) was first shown to interact with kinesin-1 light chain through biochemical binding studies (Kamal, et al, 2000) and the C-terminal region of APP, APP-C, is now a known anterograde receptor that facilitates cargo transport (Satpute-Krishnan, et al, 2006). Negatively charged beads are also known to facilitate anterograde transport (Adams and Bray et al, 1983, and Vale, et al, 1985c).

C-jun kinase interacting protein, also known as JIP-1, is a peripheral soluble scaffolding protein for the MAPK signaling pathway (Yasuda, et al, 1999). In humans, JIP-1 is found largely in the cytoplasm of cells and is widely expressed in the brain. Studies have implicated that JIP-1 interacts with and is associated with membranes via APP (Inomata, et al, 2003, and Taru, et al, 2002), and that this leads to coordinated transport of this complex (Muresan and Muresan, 2005).

Biochemical binding studies previously identified JIP-1 as a putative kinesin-1 cargo motor receptor (Verhey, et al, 2001). Studies with the Drosophila JIP-1 homologue, Amyloid precursor like interacting protein-1, or APLIP1, have implicated a 14 amino acid sequence critical for kinesin light chain binding and proper larval development (Horiuchi, et al, 2005). JIP-1 contains a 14 amino acid region that is similar

in amino acid sequence and corresponds to the 14 amino acid region of APLIP1 implicated in cargo transport in Drosophila. However, as of yet, no studies have definitively shown JIP-1 to recruit transport machinery and facilitate anterograde transport in live cells. Additionally, studies attempting to describe how multiple motile cargos might interact are lacking.

100nm fluorescent beads, chemically conjugated to the human JIP-1 14 amino acid sequence (also referred to as JIP-1 peptide) corresponding to the APLIP1 sequence implicated in proper larval development in Drosophila were injected into the squid giant axon and 100 frame 400 second videos were captured using confocal microscopy. Additionally, 100nm fluorescent beads chemically conjugated to the known APP-C anterograde receptor were injected into squid giant axons and 100 frame 400 second videos were captured using confocal microscopy. Finally, carboxylated negatively charged beads were injected into the squid giant axon and 100 frame 400 second videos were captured using confocal microscopy. All of these bead types were injected alone or with glycine-conjugated beads. Finally, negatively charged beads were injected with negatively charged beads, JIP-1 beads were injected with negatively charged beads, APP-C beads were injected with negatively charged beads, and JIP-1 beads were injected with APP-C beads. These injections were done and the resulting videos computationally analyzed by the author of this thesis in order to:

I. Test whether the 14 amino acid peptide derived from JIP-1 can recruit anterograde transport machinery in live axons.

II. Define specific properties of cargo motor receptors (charge, amino acid sequence, other) that make them suitable for transport machinery recruitment.

III. Measure using computational analysis, the biophysical transport properties of anterograde motile bead types (instantaneous, average and maximum velocity, run length and duration, pause frequency).

IV. Determine how motile beads compete or cooperate when different types are co-injected into the same axon in order to better understand how multiple motile cargos may influence each other's transport in the axon.

Chapter 2: Main Thesis

Spatiotemporal Dynamics of Transport in the Squid Giant Axon: Competition between cargo motor receptors, JIP-1, APP-C and negative charge

Pamela E. Seamster[1] and Elaine L. Bearer[1,2*]

[1]Departments of Pathology and of Neurosurgery , University of New Mexico School of Medicine, Albuquerque, NM, 87131 USA, [2]Marine Biological Laboratory, Woods Hole, 02543 MA, USA,

*Correspondence: ebearer@salud.unm.edu

*Corresponding author

Elaine L. Bearer, MD-PhD

Harvey Family Professor and Vice Chair for Research

Department of Pathology

University of New Mexico School of Medicine

MSC08 4640

1 University of New Mexico

Albuquerque, NM 87131-0001

E-mail: ebearer@salud.unm.edu

Running Title: APP and JIP-1 in Action

Key Words: Axonal transport, anterograde, APP-C, JIP-1, JIP-2, squid giant axon, confocal imaging, c-jun kinase interacting protein

Character with spaces: 36,168

Figures: 5

Tables: 0

Supporting Text: 1

Supporting Figures: 2

Supporting Videos: 6

Supporting Table: 1

Abstract

Transport of membrane-bound organelles is critical to neuronal cell function yet mechanisms hitching vesicles to transport machinery remain elusive. Here we test whether jun-kinase interacting protein (JIP-1), a peripheral membrane scaffolding protein that binds kinesin light chain, is sufficient to mediate cargo transport in axons and study its competition with amyloid precursor protein cytoplasmic domain (APP-C) and negative charge, also known motor receptors. Fluorescent beads (100 nm diameter) exhibit sequence-specific fast anterograde transport (0.46μm/s instantaneous velocity) in the squid giant axon when conjugated to a 14-amino acid synthetic peptide derived from the carboxyl terminus of JIP-1. JIP-1-beads have statistically significant faster velocities, longer run lengths, and fewer pauses of shorter durations than APP-C or negatively charged beads by cumulative probability analyses of thousands of motile beads compared by a nonparametric K-S test, with a P=0.004. In competition experiments negatively charged beads gradually cease moving when co-injected with either APP-C or JIP-1 beads, which sustain 90% motility. Co-injection of APP-C and JIP-1 beads decreases each bead's propensity to move initially. At later time points JIP-1-beads recover frequency without further decreasing APP-C moves, suggesting JIP-1 recruits motors from a cryptic pool not accessible to APP-C. Soluble JIP-1 peptide inhibits JIP-1 beads, with smaller effects on APP-C and negatively charged beads. Thus the hierarchy for recruitment of transport machinery is JIP>APP>negative charge. Organelle transport may in part be

regulated through the numbers, types and affinities of motor receptors displayed on each organelle's cytoplasmic surface.

Introduction

Fast axonal transport delivers materials synthesized in the cell body outwards within the axon to maintain and build the pre-synaptic terminus. Much is known about the molecular motors that drive axonal transport, but less about how these motors attach to cargo. Classical studies revealed the power of differential interference contrast microscopy to witness subcellular organelle movements (Brady, et al, 1982, and Schnapp, et al, 1985). When coupled with biochemical fractionation these studies resulted in the discovery of the first microtubule-based motor, kinesin-1, from squid (Vale, et al, 1985d, and Vale, et al, 1985b), later found ubiquitous in animal cells (Hirokawa, et al, 2009). Laser-scanning confocal microscopy of fluorescently-labeled particles can record dynamic movements of exogenous particles deep in the giant squid axon (Bearer, et al, 2000, Satpute-Krishnan et al, 2003, and Terasaki, et al, 1995). Exogenously delivered engineered cargo can hitchhike on endogenous transport machinery. By engineering cargo, 100nm fluorescent beads, to display a single peptide species on their surface, we demonstrated that a 15-amino acid peptide derived from the carboxyl terminus of amyloid precursor protein (APP-C) was sufficient to mediate transport in the squid giant axon, while beads conjugated to a jumbled peptide with the same amino acid composition in a different order were not transported (Satpute-Krishnan, et al, 2006).

Here we test another putative cargo-motor receptor, JIP-1, for sufficiency to mediate similar transport of fluorescent beads. JIP-1/2, a peripheral membrane scaffolding protein that tethers kinases to the cytoplasmic surface of membranes (Yasuda, et al, 1999), has been implicated as a receptor for transport: JIP-1 was identified by yeast two-hybrid screen as binding to kinesin-1 light chain (Verhey, et al, 2001); and a mutation in the Drosophila APLP1, a JIP-1 homologue, results in a kinesin-1-like transport defect in larval axons (Horiuchi, et al, 2005). This single amino acid substitution, P438L, decreases APLIP1 binding affinity for KLC in a recombinant protein pull-down assay. Intriguingly, JIP-1 also binds APP, phosphorylating it and tethering it to membrane domains (Matsuda, et al, 2001, Muresan and Muresan, 2005, Inomata, et al, 2003, and Taru, et al, 2002). Thus, our APP-C peptide may mediate transport indirectly through binding to axonal JIP-1, which secondarily binds APP to transport machinery.

We thus set out to investigate (1) whether a peptide derived from the JIP-1 domain spanning the mutation that disturbs motility in Drosophila could, like APP-C, be sufficient to confer transport capability to fluorescent beads; and (2) whether JIP-1 and APP-C interact within the context of axoplasm: do they synergize, cooperate, or compete for transport machinery? To this end, we performed a series of experiments in squid axons imaging peptide-conjugated beads in various combinations with and without soluble peptides, measuring biophysical parameters and frequency of bead movements, and comparing each peptide to deactivated beads, negatively charged beads, and beads conjugated to jumbled or mutated peptides. The picture emerges of a complex dynamic relationship between cargo

displaying different motor receptors. By titrating the amount of receptors available for motor attachments on cargo, cells could regulate transport delivery. This picture provides a mechanistic and dynamic biochemical basis for many aspects of transport function.

Results

Fast axonal transport of JIP-1 conjugated peptide-beads in the squid giant axon

To determine whether JIP-1 mediates bead transport, a peptide domain from JIP-1 spanning the highly conserved domain that includes the single amino substitution mutation that causes transport defects in Drosophila (Horiuchi, etl al, 2005) was covalently conjugated via an amide linkage to 100nm carboxylated fluorescent nanospheres (beads), leaving the normal carboxyl terminus of the protein exposed on the bead surface (Supporting Figure S1). Peptide-conjugated beads were injected together with control beads of a different color into freshly dissected squid giant axons (33pL of each bead for a total of 10^7 beads) (Supporting Figure S2a) and the bead movements recorded by time-lapse laser scanning confocal microscopy (Figure 1, Supporting Videos S1-3).

JIP-1 bead movements resemble those of APP-C beads as we previously reported (Satpute-Krishnan, et al, 2006). Imaged on the anterograde side of the injection site, JIP-1 beads move rapidly anterograde (Figure 1a upper panel, d and g; Supporting Video S1), as do APP-C conjugated beads (Figure 1b, upper panel; e and i; Supporting Video S2). No significant movement is observed on the retrograde side

of the injection site. Negatively charged particles have long been known to transport in axons (Terasaki, et al, 1995, and Adams and Bray, 1983). Since we conjugated peptides to carboxylated beads that carry a negative charge such as might bind kinesin (Vale, et al, 1985c), we also studied the behavior of unconjugated beads. As expected, similar anterograde motility is also found for washed carboxylated (negatively charged) beads (Figure 1c, upper panel, f and k; Supporting Video S3). Hence, as one control we conjugated glycine to carboxylated beads using the same amide linkage as for peptide conjugation. We reasoned that glycine, a small amino acid, would present a carboxylic acid group to the cytoplasm as does the peptides, but without the intervening amino acids. Glycine conjugation quenches the beads' ability to transport, demonstrating that our chemistry for conjugating negatively charged beads to peptides eliminates their ability to recruit active kinesins, and further that the carboxylic acid moiety of a single amino acid is not sufficient to mediate bead transport (Figure 1a, b and c, lower panels, h, j, and l; and green beads in Supporting Videos S1-3). Glycine-conjugated beads remain stationary even when co-injected with rapidly motile JIP-1, APP-C, or negatively charged beads in the same axon, regardless of which color of bead was conjugated to the glycine, peptides, or simply carboxylated.

Higher magnification images showing the positions of single beads in each frame of a 4sec 100 frame time-lapse sequence demonstrate apparent similarity between step sizes of each bead type (Figure 1d, e, and f respectively). Kymographs also show similar slopes for those beads that continue to move throughout the sequence, as if they go at similar rates (Figure 1g), although JIP-1 beads may move

slightly more rapidly. Notably immotile glycine beads produce vertical lines in the kymograph as their position does not change over time.

JIP-1-beads transport better than APP-C- and negatively charged beads

All three motile bead types (JIP-1, APP-C and negatively charged beads) exhibit average instantaneous velocities consistent with fast axonal transport, with JIP-1 at $0.46 \pm 0.17\mu m/s$, APP-C beads at $0.44 \pm 0.17\mu m/s$, and negatively charged at $0.35 \pm 0.15\mu m/s$ (Figure 2a, Supporting Table 1).

More detailed comparisons of thousands of motile beads from 10 different axons when on their own or co-injected with immotile beads, reveal that bead types differ in run velocity, run length and pause duration. Cumulative probability analysis of velocities detect significant differences between JIP-1 beads and the other two beads types, with a two-sample nonparametric Kolmogorov-Smirnoff test (K-S test) showing that the probability of the null hypothesis (that the data are from a continuous distribution) is $P<0.004$ (Figure 2b). Other aspects of bead behavior also differ significantly for JIP-1 compared to APP-C and negative change. Run lengths of JIP-1 beads are longer (Figure 2c), and JIP-1 beads' pause durations are shorter (Figure 2d and Supporting Table S1). JIP-1 beads spend half as much time stalled as APP-C and negatively charged beads (Figure 2e). These differences between JIP-1 beads and the other two bead types are significant by the K-S test to a $P=0.004$, while the difference between APP and negatively charged beads for run length and pause duration are insignificant.

Another way to compare efficiency of bead transport is to quantify ratios of moving to stationary beads. By dividing our 100-frame video sequences into 10-frame sets, we analyzed the proportion of beads moving in each set throughout the sequence (Supplemental Fig. S2b). A high proportion of JIP-1 beads move, ~ 90%, when co-injected with immotile glycine beads, which show infrequent moves, ~5 % (Figure 3a). Similar frequencies of movements are observed for either APP-C beads or negatively charged beads co-injected with immotile glycine-beads.

JIP-1 bead motility is sequence specific. The single amino acid substitution in the Drosophila mutant, P438L, that decreases organelle movement (Horiuchi, et al, 2005) also renders the JIP-1 peptide incapable of mediating anterograde transport of beads (Figure 3b, Supporting Figure S1 and Supporting Video S4). Mutant peptide bead motility decreases from 90% seen for wild-type to 5-10% for mutant peptide in the same axon. This demonstrates specificity of JIP-1 peptide sequence for anterograde transport, and validates our assay as being consistent with the behavior of full-length JIP-1 protein *in vivo*.

APP-C and JIP-1 are not merely interacting via a negative charge with transport machinery. Motile APP-C, negatively charged (carboxylated) beads and immotile glycine beads all have a pI ranging from 4.3-5.95 (charge of -1 at neutral pH), while for motile JIP-1 and immotile mutated JIP-1, the pI is identical, pI = 2.9 (charge of -4). Hence pI and charge do not correlate with motility.

Competition between bead-conjugates for transport machinery

To determine whether all three motile bead types share similar transport machinery we developed a competition assay. We reasoned that beads that use the same equipment would compete for scarce machinery as detected by decreased percentage of beads moving, whereas beads that use different motors would not affect each other's motility. First we injected two differently colored beads of the same type, red and green negatively charged beads, which effectively doubles the number of motile beads injected over previous experiments. Transport efficiency decreases similarly for each color, from 90% when with an immotile bead to 50% with an equivalent motile bead (Figure 3c, Supporting Video 5). Thus red and green beads are functionally similar; and the amount of transport machinery is finite and saturable under the conditions of our bead experiments.

We then co-injected peptide beads with negatively charged beads, aiming for a bead volume at which 90% of both beads would move at the start of imaging to reveal time-dependence of any decrease in frequency of moves. When co-injected with negatively charged beads all bead types start out at 90% motile. Over the 400 sec recording, both JIP-1 and APP-C beads maintain ~90% motility, while co-injected negatively charged beads drop over 400s from the initial 90% to ~10% motile (Figure 3d, e). Negatively charged beads lose motility steadily at a rate of 0.225% and 0.213% per second when co-injected with JIP-1 and APP-C respectively. This result was reproducible regardless which colors of beads were used. Thus by the end of the recording, active motors initially available for negatively charged

bead motility have become unavailable, likely adsorbed more specifically and tightly to the peptide beads and thus removed from the soluble pool.

To arrive at an estimate of the relative affinity of these different beads for transport affinity, we performed some calculations. Based on the number of COOH residues per bead, predicted size of conventional kinesin, and bead surface area, we found that each bead could accommodate a maximum of 1200 motors. With an injected bead amount of 10^7, this gives a total binding capacity of 1.2×10^{10}. The concentration of monomeric conventional kinesin heavy chain protein in the axon is estimated at 0.5 µM (Brady, et al, 1990), or 0.25 µM for the holoenzyme. If the volume of axoplasm within which the beads are moving is assumed to be a rectangle with the short sides the diameter of the plume and the length the distance of bead trajectory during the video sequence, and if conventional kinesin were the only motor available, 10^{14} molecules would be present in the volume of axon occupied by the beads, which exceeds bead binding capacity by a factor of 10^4. In addition at least two anterograde motors other than conventional kinesin are also expected in the axon, members of the heterotrimeric kinesin 2 family and kinesin 3 (DeGiorgis, et al, 2008). Why then do the negative beads stop moving? Some of these motors may be inactive, and others bound to endogenous transport organelles, invisible in these experiments. At the point when the negatively charged beads are no longer motile, the amount of available and active transport machinery cannot exceed the maximum number of binding sites on transporting peptide-beads, ie $\sim 10^{10}$. Hence peptide-beads compete successfully with negative charge for the limited active

transport machinery in axoplasm, probably via more specific and higher affinity binding or by activating motors.

A next question is how JIP-1 and APP-C beads compete when co-injected. Like co-injected negatively charged beads, JIP-1 and APP-C beads reduced each other's motility frequency by >50% when co-injected (Figure 3f and Supporting Video S6). JIP-1's transport frequency decreases to ~40%, and APP-C's to ~30% when co-injected as opposed to 90% when injected alone or with either non-motile beads (glycine) or negatively charged beads. Later in the recording session a curious phenomenon occurs--JIP-1 beads recover transport, from 40% to 70%, while APP-C bead motility remains at ~30%. Thus JIP-1 may recruit a new motor from a cryptic motor pool not accessible to APP-C beads, such as tightly-associated motors on the endogenous transport vesicles (Schnapp, et al, 1992, and DeGiorgis, et al, 2008).

Soluble JIP-1 peptide inhibits JIP-1 bead transport

Previous reports have suggested that APP and JIP interact to tether motors, specifically conventional kinesin, to transport vesicles (Matsuda, et al, 2001, Muresan and Muresan, 2005, and Inomata, et al, 2003). In this scenario APP-C-beads might recruit soluble JIP-1 from the squid axoplasm and mediate transport via secondary interactions with motors. To test this we injected soluble JIP-1 peptide containing the motor binding domain into the axon together with JIP-1 and APP-C beads (Figure 4). This peptide would be expected to bind transport machinery via its JIP-1 binding domain, and thus compete with JIP-1 peptide on beads or JIP-1

recruited to beads by APP-C. To control for the effects of peptide injections on transport we performed two control experiments: Injection of a jumbled JIP-1 peptide with the same amino acid composition but in a random order; and injection of JIP-1 peptide together with both colors of negatively charged beads. Jumbled JIP-1 had only a marginal effect on JIP-1 bead transport, and, as expected, negatively charged beads were also not affected by soluble JIP-1 peptide, as they likely bind motors non-specifically via electrostatic interactions and not via JIP-1 binding sites.

Soluble JIP-1 peptide had a strong effect on JIP-1 bead movements, which dropped from 70% motile to 20% motile at even the lowest concentration of soluble peptide (0.16µg/µl). APP-C beads in the same axon showed little change at this peptide concentration. Thus, at least some of the pool of transport machinery recruited by JIP-1 is different from that recruited by APP-C, which appears to recruit about 30% of its machinery independent of JIP-1.

Discussion

Live cell confocal imaging of fluorescently-labeled microspheres injected in the squid giant axon has led to our identification of a second cargo-motor receptor in addition to APP-C, JIP-1. Our studies using engineered cargo displaying a single peptide species definitively show that single peptides are sufficient to hitch cargo to motors for transport (Satpute-Krishnan, et al, 2006), an experiment difficult to perform with fluorescently labeled proteins expressed inside cells where other cellular components would also populate the organelle membrane and contribute to

transport. The amino acid sequence of the JIP-1 domain is highly conserved across species, with 8 of the 14 residues identical between human, fly and worm (Horiuchi, et al, 2005), suggesting an evolutionary conserved role of this sequence, such as in cellular transport.

By measurements of various parameters of bead transport, JIP-1 beads display increased velocity, longer run lengths and shorter pauses. JIP-1's transport efficiency over other cargo-motor receptors, APP-C and negative charge, was further revealed in competition experiments. Although both JIP-1 and APP each out-compete negatively charged beads, JIP-1's movements are more robust than APP-C when the two peptide-beads were co-injected. Finally soluble JIP-1 peptide inhibits JIP-1 beads more than APP-C, suggesting that the two cargo-receptors share some motors and individually prefer other, possibly different, motors. Thus APP-C is not only a binding site for the scaffolding protein JIP-1, but also recruits motor machinery independently of JIP-1.

These results lead to a more complex picture of cargo-transport than previously imagined. With 45 kinesins in the human and mouse genome (Hirokawa and Takemura, 2005) many motors would be expected involved in transport. Adding further complexity the microtubule tracks may also differ through either post-translational modification of the tubulin subunit altering motor preference (Hammond, et al, 2010), or by complexing with different forms of tau protein (Kanaan, et al, 2011). Now we show a multiplicity of cargo motor receptors with similar and differing apparent motor preferences (see Diagram in Figure 5). This plethora of competing players will likely need both modeling and detailed

biochemical analysis to delineate such that the full picture of transport regulation

may emerge.

Materials and Methods

Preparation of beads

Carboxylated fluorescent nanobeads, 100 nm in diameter, with red (580/605nm) (Fluospheres, Invitrogen) or green (480/520nm) fluorescence (Bangs Laboratories) were washed through a Low Binding Durapore filter (100 nm cut-off, Millipore). Uncoated negatively charged beads were washed and diluted to 2% in motility buffer and used for injection without further treatment. Synthetic peptides ordered directly (APP-C, Biodesign, Inc www.biodesign.com) or custom synthesized (Aves Labs, Inc www.aveslab.com) based on protein sequences from Genbank. For JIP-1, we selected a 14-amino acid sequence from JIP-1, also found in JIP-2 (JIP-1/2) that spans a single amino acid substitution found in a mutant Drosophila JIP, APLIP-1, that affects kinesin light chain-binding (Horiuchi, et al, 2005). Conjugations were performed as described (Satpute-Krishnan, et al, 2006). Briefly, 10 µl of carboxylated beads were washed in water. Peptides (20 µl of a 2mg/ml stock) were added to the pellet of washed beads, conjugated via their amino terminus to carboxylated beads using 1-Ethyl-3-[3-dimethylaminopropyl]carbodiimide hydrochloride (EDAC) in the presence of Sulfo-NHS (Thermoscientific,

http://www.piercenet.com/Objects/View.cfm?type=ProductFamily&ID=02030312). The conjugation reaction was quenched with ethanolamine or glycine. Glycine-conjugated beads were prepared in parallel without peptide and quenched with glycine. We also tested ethanolamine quenched beads subjected to EDAC and SulfoNHS in the absence of peptide. These displayed no transport capability when injected into the axon.

Dissection and Microinjection of Squid Giant Axons

The giant axon was dissected from squid (*Loligo pealei*) freshly caught at the Marine Biological Laboratory (MBL), Woods Hole, MA (Bearer, et al, 1993). Squid were used within 36 hours of procurement from the ocean as they do not survive long in captivity. Red and green beads (30-65 pL of a 2% bead solution containing 10^7 beads with 1200 binding sites per bead based on the number of conventional kinesins that the surface area of the bead can accommodate), either un-conjugated (negatively charged), conjugated to a peptide or to glycine, were mixed in equal amounts and then loaded into a mercury micropipette (Jaffe and Terasaki, 2004, and Satpute-Krishnan, et al, 2006). Injection volumes were controlled by direct observation during injection with 10x phase objective lens in an upright Zeiss Axioscope. The diameter of the injectate within the axon was measured using a micrometer reticle to monitor consistency between injections.

Imaging by Confocal Microscopy

Immediately after injection, axons were transferred to an imaging chamber filled with calcium-magnesium-free artificial seawater, and the chamber carried to the Zeiss 510 laser-scanning confocal microscope at the MBL. After capture of an initial image of the injection site at 10x, 100 frame 4 second time lapse sequences were recorded using a 40X Achroplan 0.8NA water correctible objective which has a long working distance and does not squash the axon. Axons are typically 0.8-1 mm in diameter and 7 cm in length. The injection site was placed 2-3 cm along the axon

27

towards the pre-synaptic termini from the ganglion containing the axonal cell bodies, and 0.4 mm deep to the surface. Because of the translucency of the squid axon, beads were readily detected even at this depth with a 45-50 μm optical section with 488 and 543 laser excitations, band pass filters 500-530 and 565-615 respectively using the Zeiss confocal multi-tracker function for simultaneous collection of red and green channels. Multiple sequential recordings were collected from each axon, and the time between injection and each sequence recorded. Typically the time between injection and imaging was 8-12 min and bead movements began to slow 50 min after mounting in the confocal microscope. Sequences selected for analysis were only compared when taken from the same time interval after injection. Shown are representative examples of 17 different axons from a total of 47 successful injections acquired over a period of three summer seasons.

Analysis of Transport

Bead movements were analyzed using Metamorph 7.0r1 (Molecular Devices, http://www.moleculardevices.com/pages/software/metamorph.html). First the frames of each video were aligned based on the grayscale phase image of the axon. Then an area within the frames containing >50 individual beads, omitting the area around the injection site where axoplasmic integrity is disturbed and many beads are found in aggregates that do not move. The cropped aligned sequence was then subdivided into ten frame increments. Individual beads in the first frame of each ten frame increment were counted. Then using "Stack Arithmetic" function in

Metamorph, a single image of all ten frames was produced, generating streaks for each moving bead and dots for stationary beads (Supporting Figure S2b). Streaks within this time-lapse image measuring > 1.5 μm were considered moving beads. We chose a cut-off of 1.5 μm as the minimal distance a bead must move to qualify as moving. Dividing the number of streaks by the total number of beads in the first frame gives the ratio of beads moving. For velocity the distance between moves for each moving bead was measured. Only beads moving consistently in one direction with a step size greater than 1.5 μm/4sec time lapse, into and out of a frame were included. MatLab Statistical Toolbox (Mathworks http://www.mathworks.com/products/matlab/) was used to create probabilistic graphs, and apply Kolmogorov-Smirnov test of the null hypothesis (Andrews, et al, 2009).

AUTHOR CONTRIBUTIONS

P.E.S. analyzed experiments and wrote the first draft. E.L.B. designed, performed and analyzed experiments. P.E.S. and E.L.B. prepared the manuscript.

COMPETING FINANCIAL INTERESTS

The authors declare no competing financial interests.

Figure Legends

Figure 1. Fast anterograde transport of JIP-1 resembles transport of APP-C and negatively charged beads in the squid giant axon.

(**a, b, c**) Images of stack arithmetic from representative video sequences of axons doubly injected with (a) JIP-1; (b) APP-C, and (c) negatively charged red beads (top panels) and green glycine-quenched beads (a-c, lower panels). For each series, left panel, 0s (frame 1); middle panel, 200s (frames 1-50), and right panel, 400s (frames 1-100). See Supporting Videos 1, 2, and 3. White arrows in lower panels of (a), (b), and (c) indicate non-motile glycine beads over 100 frame videos.

 (**d-f**) Individual bead movements. An individual JIP-1 bead (blue arrow) is displayed at higher magnification in (d); APP-C bead (yellow arrow) displayed at higher magnification in (e); and negatively charged bead (purple arrow) displayed at higher magnification in (f).

(**g - l**) Kymographs of JIP-1 (g) and glycine beads (h) in the same axon; APP-C (i) and glycine beads (j) in another axon; and negatively charged (k) and glycine beads (l) together in a third axon.

Figure 2. Measurements of transport dynamics of JIP-1, APP-C, and negatively charged beads

(**a**) Histogram showing number of moves at each velocity for the three different bead types as indicated (JIP-1, n=357; APP-C, n=433), and negatively charged, n=413).

31

(b-d) Cumulative probability analyses of JIP-1, APP-C, and negatively charged beads when injected alone or with an immotile bead (glycine).

(b) Velocity; K-S test results: JIP-1 vs. APP-C, P=0.004; JIP-1 vs. negatively charged, P=0.0004; APP-C vs. negatively charged, P=0.7.

(c) Run length. K-S test: JIP-1 vs. APP-C, P=0.0038; JIP-1 vs. negatively charged, P=0.0004; APP-C vs. negatively charged, P=0.78.

(d) Pause duration. JIP-1 was 9.69+/- 12, APP-C 14.8+/-24, and negatively charged 17.3+/- 23 sec/pause. K-S test: JIP-1 vs. APP-C, P=0.0075; JIP-1 vs. negatively charged, P=0.0021; APP-C vs. negatively charged, P=0.5161.

(e) Percentage of time spent paused for all three beads types.

See Supporting Table S1 for statistics. JIP-1 bead analysis: 3 axons, 4 videos, 32 beads, 1677 total moves, and 8956 seconds of total time; APP-C bead analysis: 4 axons, 5 videos, 41 beads, 1648 total moves, and 12656 seconds of total time; Negatively charged bead analysis was of 3 axons, 5 videos, 45 beads, 1522 total moves, and 12536 seconds of total time.

Figure 3. Frequency of moves reveals competition between bead types

(a) Percentage of beads moving for JIP-1 (red) and glycine (green) beads in a representative 100-frame video captured at 4 sec intervals and measured at 10 frame increments.

(b) Percentage of beads moving in a representative axon co-injected with JIP-1 and mutated JIP-1 beads (P→L) and counted in 10 frame increments (see Supporting Video 4).;

(c) Negatively charged beads of either red or green compete equally. Frequency of moves of negatively charged beads red and green negatively charged beads co-injected in a single axon. (See Supporting Video 5)

(d-e) Competition between JIP-1 (d) and APP-C (e) with negative charge beads for transport.

(f) Competition between JIP-1 and APP-C beads over 400 frames (1600s sequence). Cumulative probability analysis shows no change in run lengths or pause durations between APP-C and JIP-1 beads injected together versus when injected singly with glycine beads (Supporting Videos 6).

Figure 4. Soluble JIP-1 peptide interferes with JIP-1 bead transport

Soluble synthetic JIP-1 peptide was co-injected with a mixture of red and green JIP-1 and APP-C beads, or red and green negatively charged beads as indicated. Transport of beads was imaged in 100 frame 4s time-lapse confocal microscopy sequences. Experiments were performed in triplicate alternating bead colors for each peptide. Frequency of moves from first and last 10 frames of representative 100-frame video are shown at each peptide concentration.

Figure 5. Diagram of motor-bead competition

Hypothetical motor recruitment by JIP-1 (green) and APP-C (red) beads. JIP-1 and APP-C beads initially compete for the soluble pool of anterograde machinery (soluble motor 1), most likely consisting of kinesin-1, which is abundant and soluble in axoplasm (Brady, et al, 1990), and possibly other anterograde transport machinery such as kinesin-73 (Huckaba, et al, 2011). The gradually increasing

frequency of JIP-1 beads when in competition with APP-C beads, as shown in Figure 3f, suggests that an additional motor not readily available (organelle bound motor 2) selectively prefers JIP-1 over APP-C. This "organelle motor 2" may include those motors tightly associated with organelles (yellow) (Schnapp, et al, 1992), such as kinesin-3, known to be present in squid axons, with a small soluble component and a large component tightly associated with axoplasmic organelles (DeGiorgis, et al, 2008).

Supporting Figure Legends

Figure S1 Sequences of peptides and diagrams of their orientation after conjugation to beads as used in co-injection experiments. Each peptide was uniquely conjugated to one or the other color of beads such that the specificity of each peptide for transport could be observed. Soluble peptides were also injected for some experiments.

Figure S2 Similar amounts of each color bead injected and how percent beads moving was determined from time-lapse video sequences and (a)(a1) Shows a phase image of the oil droplets in the axon. (a2) Multichannel image or both colors of beads and the oil droplets. Yellow indicates overlap of red and green fluorescence. (a3) and (a4) Separation of color channels shows the volume of injection of both green and red color beads. (b) (b1-3) Red JIP-1 beads, and (b4-6) Green glycine beads. (b1) Red channel showing individual frame 1; (b2) individual frame 10; and (b3) frames 1-10 stacked of JIP-1 beads. Dotted lines in (b3) represent beads moving during the 10 frames. (b4) Green channel showing individual frame 1; (b5) individual frame 10; and (b6) frames 1-10 of glycine beads. Minimal numbers of dotted lines in (b6) indicate rare glycine bead movement over these ten frames. Measuring the distance between the dots also allows determination of the velocity of bead movement. Also see Methods and Supporting Videos. Low magnification multi-channel image taken immediately after injection demonstrates that similar volume of beads are present at the injection site, marked by two oil droplets that were loaded into the micropipette on each side of the bead

35

volume.

Supporting Video S1. JIP-1 and Glycine. JIP-1 conjugated beads move briskly in the axon. JIP-1 conjugated beads (red) were co-injected with an equal volume of glycine conjugated beads (green) and imaged by time-lapse laser-scanning in confocal microscopy with one frame every 4 sec for one hundred frames (400 sec). After alignment of the gray scale background, playback is at 24 frames per second. The time stamp and magnification bar are embedded in the raw sequence and were not aligned. JIP-1 conjugated beads (red) display robust movement, while glycine conjugated beads (green) remain stationary. (See Figure 1a).

Supporting Video 2. APP-C and Glycine beads. APP-C beads move rapidly in the axon. Video sequence captured with same parameters as Video 1, with APP-C (red) substituted for JIP- 1 co-injected with glycine beads (green). (See Figure 1b).

Supporting Video S3. Negatively charged and Glycine beads. Negatively charged beads (red) facilitate movement, while glycine conjugated beads (green) do not. Video captured and displayed as for Video 1 (See Figure 1c).

Supporting Video S4. JIP-1 wild-type and JIP-1 P438L. Video sequence of JIP-1 conjugated beads (red) co-injected with JIP-1 (PàL) conjugated beads (green). The video was captured and displayed with the same parameters as Video 1. JIP-1 conjugated beads (red) are motile, while beads conjugated to JIP-1 with a single amino acid substitution (PàL) (green) are severely reduced in their movement. (See Figure 3b).

SupportingVideoS5. Negatively charged red and green beads. Both red and green beads move similarly when displaying similar surfaces. Video captured and displayed as for Video 1. (See Figure 3c).

SupportingVideoS6. JIP-1 and APP-C in the same axon. Top sequence: JIP-1 (green) and APP-C (red) in frames 1-100. Video was captured as for Video 1 except 400 frames at 4 frames per second over 1600 seconds was captured. About 40% of the JIP-1-beads (green) display motility while only 30% of the APP-C-beads (red) display motility. (See Figure 3f). Bottom: The same axon, at later time points (frames 301-400, 1200-1600 sec). This sequence is the last 100 frames from the same video as in the top video. Note that JIP-1 conjugated beads (green) have increased to 70% motility from 40% (also see Figure 3f), while APP-C conjugated beads (red) have remained at a constant 30% motile.

Figure 1

Figure 2

Figure 3

a. JIP-1 vs Glycine — FVEYTCPTEDIYLE / G

b. JIP-1 (Pro) vs JIP-1 (Leu) — FVEYTCPTEDIYLE / FVEYTCLTEDIYLE

c. Negative Charge vs Negative Charge

d. JIP-1 vs Negative Charge — FVEYTCPTEDIYLE

e. APP-C vs Negative Charge — GYENPTYKFFEQMQN

f. JIP-1 Beads vs APP-C Beads — FVEYTCPTEDIYLE / GYENPTYKFFEQMQN
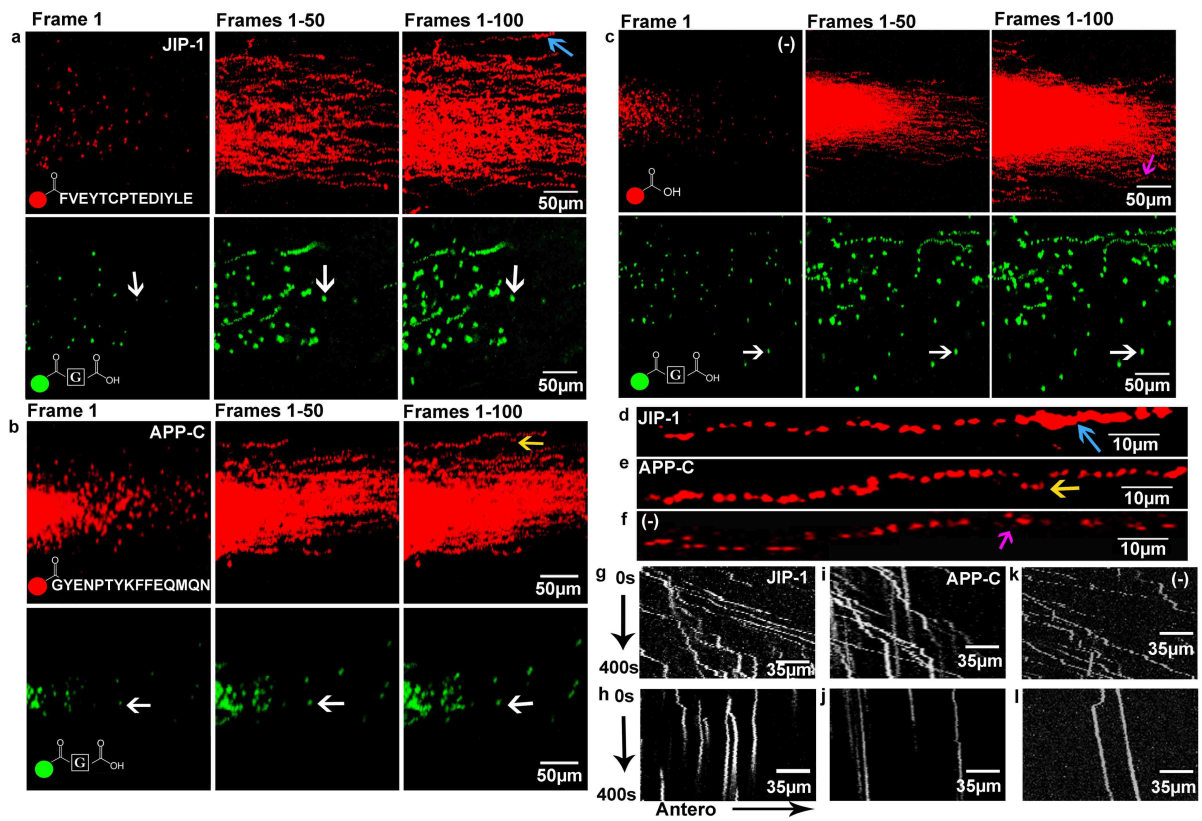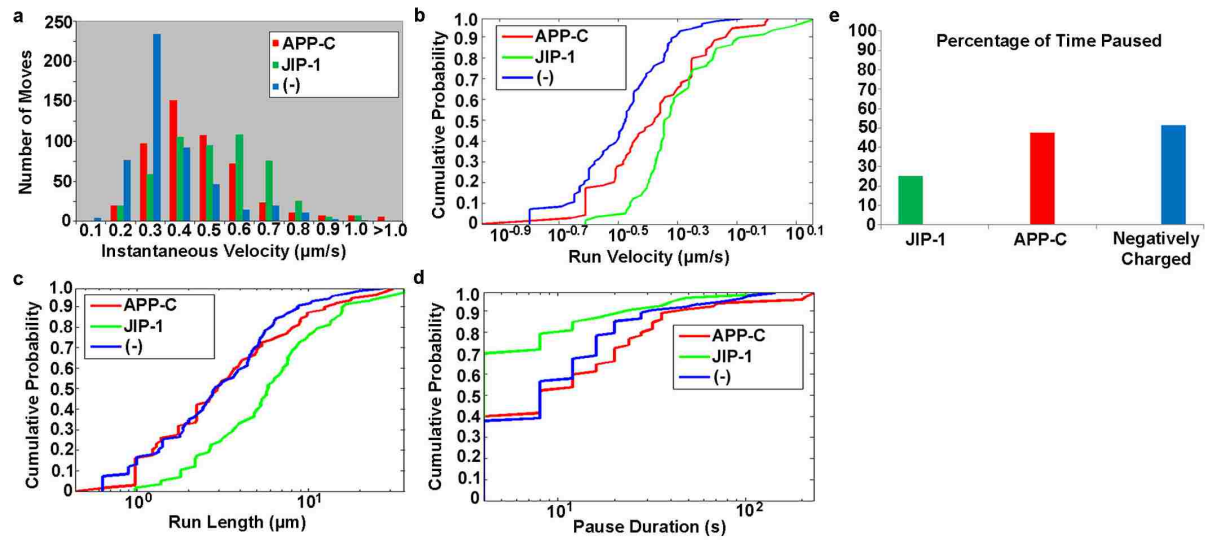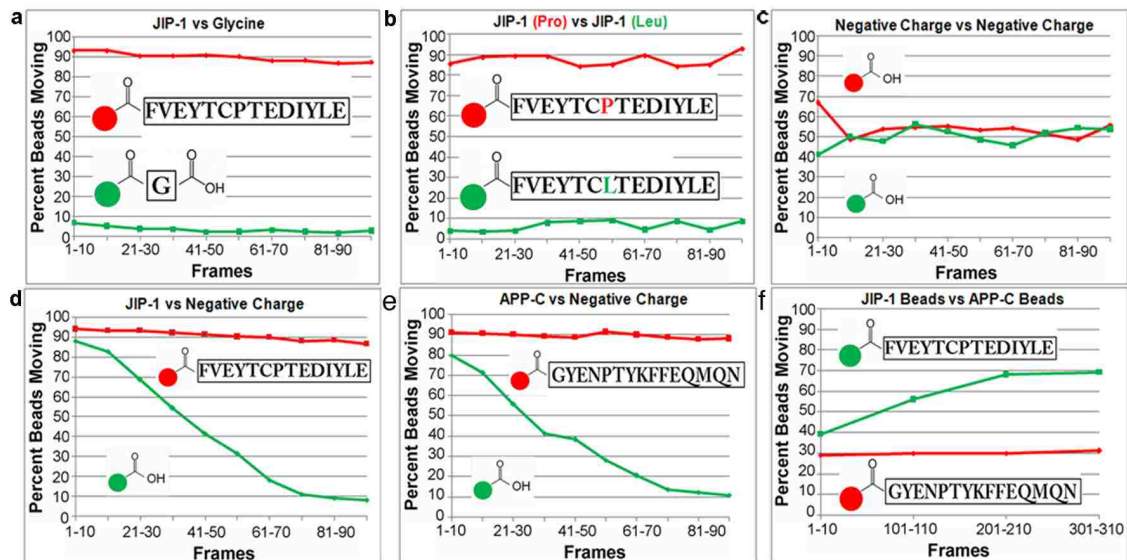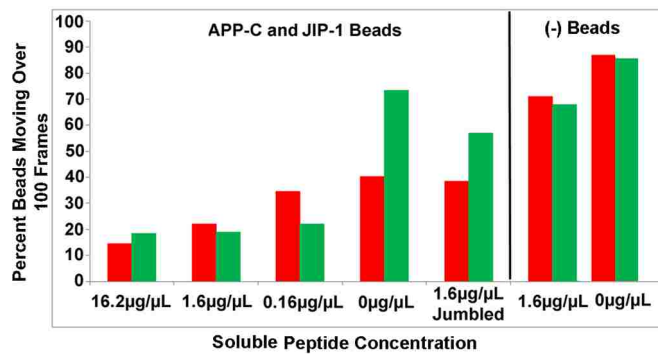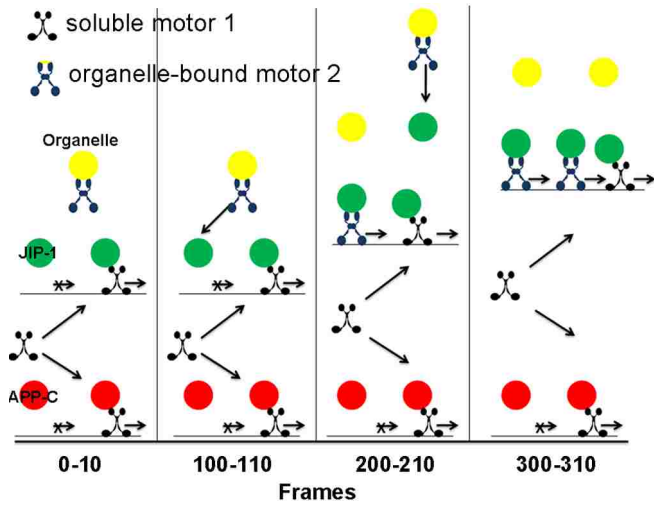
Figure 4

Figure 5

Supporting Figure 1

Peptide	Sequence	pI	Charge
Carboxylic Acid (negative charge)	-COOH	5	-1
Glycine	$-NH-CH_2-COOH$	5.97	Neutral
APP-C	$_{681}GYENPTYKFFEQMQN_{695}$	4.3	-1
JIP-1	$_{698}FVEYTCPTEDIYLE_{711}$	2.9	-4
JIP-1 (Leu Substituted)	$_{698}FVEYTCLTEDIYLE_{711}$	2.9	-4
JIP-1 (Jumbled)	$_{698}LEIPFEVDYTECTY_{711}$	2.9	-4
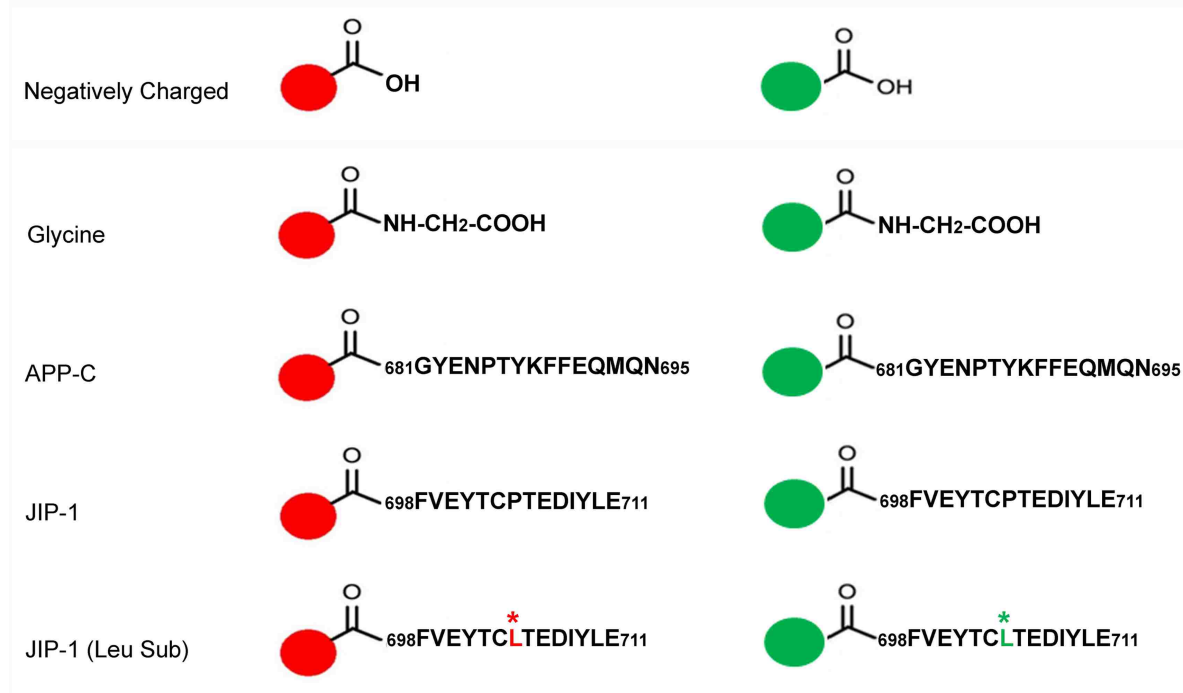
Supporting Figure 2
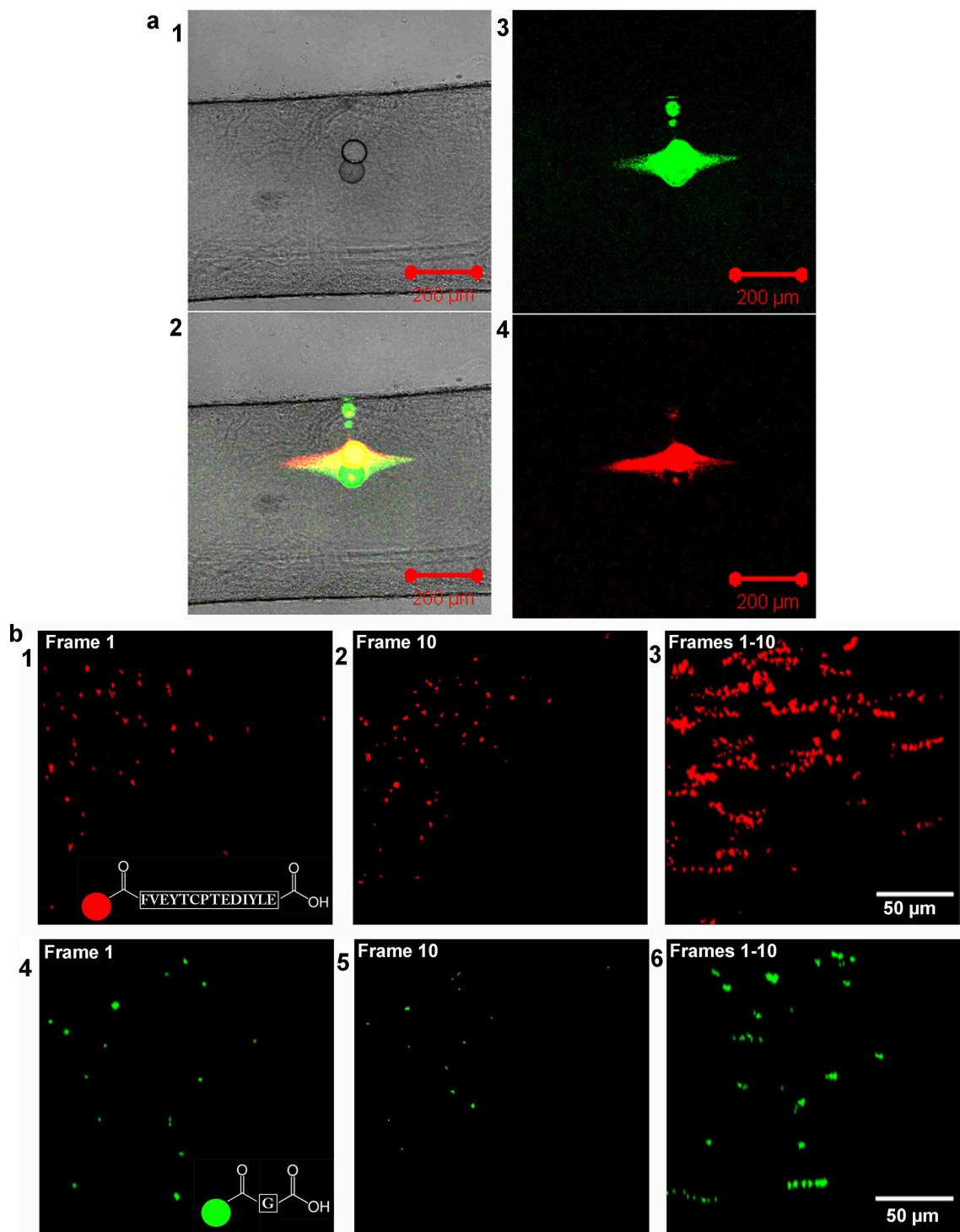
Supporting Table 1

Transport measurements of JIP-1, APP-C, and negative charged beads.

Bead	Instant. Velocity (μm/s)	Maximum Velocity (μm/s)	Average Run Length (μm/run)	Average Run Duration (s/run)	Average Run Velocity (μm/s)	Total % Time Paused	Avg. Pause Duration (s/pause)
JIP-1 (n=32)	0.465 ± 0.170	1.863	11.95 ± 16.61	25.70 ± 32.27	0.438 ± 0.160	25.1	9.69 ± 12.35
APP-C (n=41)	0.440 ± 0.176	1.757	6.58 ± 7.42	14.96 ± 15.76	0.428 ± 0.143	47.2	14.83 ± 24.40
Negatively Charged (n=45)	0.350 ± 0.157	1.579	5.16 ± 5.90	14.78 ± 15.06	0.336 ± 0.0980	51.4	17.28 ± 23.51

Chapter 3: General Discussion

The regulation of cargo transport in the axon is critical for proper development, maintenance and function (Sau, et al, 2011). However, the exact mechanisms by which the axon is able to regulate and coordinate this transport are poorly understood. The above study has presented multiple insights into how cargo is selected for transport and how transport is regulated.

JIP-1, a scaffolding protein sufficient to recruit the anterograde motor machinery that drives transport in a heterologous engineered cargo/squid axon assay

First, through computational analysis, the identification of a 14 amino acid JIP-1 peptide as an anterograde cargo transport receptor adds to the list of already known anterograde receptors, APP-C and negative charge. A JIP-1 peptide similar to the 14 amino acid peptide used for my analysis has been shown to interact with kinesin-1 *in vitro* (Verhey, et al, 2001 and Horiuchi, et al, 2005), and an amino acid region from the JIP-1 homologue APLIP1 that corresponds to the 14 amino acid peptide used in my analysis has been shown to influence vesicle transport and development in Drosophila (Horiuchi, et al, 2005). While these previous studies suggested that this JIP-1 peptide is involved in kinesin-1 mediated anterograde vesicular transport, the study I have presented is the first to definitively show active anterograde transport of JIP-1 peptide associated vesicles in a live cell.

The study I have presented is also the first to describe in depth some properties of anterograde cargo motor receptors. Lack of transport of glycine conjugated beads and

lack of transport of mutated JIP-1 peptide beads reveal that a terminal carboxylic acid residue on a peptide sequence and negative charge of a peptide sequence alone are not sufficient characteristics of a cargo motor receptor to facilitate transport. Additionally, I observed none of these bead types transporting in the retrograde direction. This brings up the interesting possibility that I have identified characteristics for anterograde motor receptors, and that there are entirely different characteristics of receptors for retrograde transport.

JIP-1 peptide, APP-C and negatively charged beads all display instantaneous velocities (0.1-0.5microns/sec) (Vale, et al, 1985a, and Lasek and Brady, 1985), and maximum velocities (1-5microns/sec) (Allen, et al, 1982 and Brady, et al, 1982b) consistent with fast axonal transport mediated by kinesin-1. However, JIP-1 peptide beads pause less frequently and for shorter durations than APP-C and negative charge beads, have faster run velocities, and are overall, more efficient at transport. Fast and slow axonal transport are both thought to be carried out by kinesin-1, yet differ in the frequency of and duration of pauses. This provides an interesting possibility that the way a cargo is able to interact with transport machinery determines how efficiently it will be transported. While JIP-1 peptide, APP-C and negatively charged beads all display fast axonal transport, the increased pause frequencies of APP-C and negative charge beads compared to JIP-1 peptide beads suggest that JIP-1 peptide is better able to sustain interactions with the transport machinery, in this case kinesin-1, having a lower 'on/off' rate. APP-C beads pause less frequently and for shorter durations than negative charge beads, and thus it is likely APP-C has a lower 'on/off' rate with the transport machinery (kinesin-1) than negative charge.

Various other, equally plausible, explanations for the data in light of other published results are: 1) different isoforms of kinesin-1 light chains expressed in axons may have different interactions with JIP-1 peptide, APP-C, and/or negative charge, therefore affecting transport behavior of these cargos, 2) different post-translational modifications of microtubules cause different processivity of motors carrying JIP-1 peptide beads, APP-C or negative charge beads and therefore affect the transport behaviors of these cargos, 3) APP-C and negative charge beads may be using a different motor for transport than JIP-1 peptide beads, and 4) other anterograde kinesin motors, such as kinesin-2, are used for transport and have different interactions with JIP-1 peptide, APP-C, and negative charge cargo motor receptors.

While the 'on/off' rate of a receptor with kinesin-1 is one possible explanation for the observed increase in pause duration and frequencies of APP-C and negative charge beads compared to JIP-1 peptide beads, there are other factors that may account for and/or contribute to these observed pauses. JIP-1 peptide, APP-C, and negative charge have all been shown to interact with kinesin-1 light chain (Verhey, et al, 2001, and Kamal, et al, 2000). Kinesin-1 has three isoforms of kinesin light chain (Stenoien and Brady 1997, and Muresan, 2000), and the expression of these isoforms in the axons I analyzed is indeterminate. It is possible that in the axons I have analyzed, there is an isoform that is more specific for interactions with JIP-1 peptide and APP-C, causing these bead types to have lower 'on/off' rates with the machinery than negative charge beads. However, given that I analyzed multiple axons and similar results were attained from all, it is not likely the isoform of kinesin-1 light chain expressed is responsible for the

differences in cargo interactions with motors that result in the different pause frequencies and durations.

Another possibility is that the microtubules on which APP-C and negatively charged beads are transporting have undergone modifications that make the kinesin motors transporting them less processive (Hammond, et al, 2010), while the microtubules on which JIP-1 peptide beads are being transported have not been modified. However, I observed similar pause frequencies for JIP-1 peptide, APP-C, and negative charge beads across multiple axons, making the likelihood of similar modifications of microtubules on which only APP-C and negatively charged cargo are being transported across multiple axons improbable. This indicates the pause frequencies and pause durations of JIP-1 peptide, APP-C and negative charge beads are phenomena that are due to the cargo motor receptor, and not modifications of microtubules.

One more possible explanation for the observed increase in pause frequencies and durations of APP-C and negatively charged beads is that they are using a less processive unidentified motor for transport. However, this is likely not the reason for the observed increase in APP-C and negatively charged bead pause durations and frequencies due to the competition experiments showing JIP-1 peptide beads and APP-C beads outcompeting negative charge beads for transport. This competition indicates that all three cargo-bead types share the same motor. If all three bead types share the same motor, and the pause durations and frequencies of APP-C and negative charge beads were caused by transport by a less processive motor, I would expect JIP-1 peptide beads, sharing this motor, to pause more frequently as well. Taken together, the indications are that JIP-1 peptide, as a cargo motor receptor, sustains interaction with the transport

machinery better than APP-C and negative charge making it a more efficient cargo motor receptor for transport.

Finally, the presence of other anterograde kinesin family motors in axons raises the question of whether the beads are using several different motors for transport. Due to the transport rates of the beads, I attributed the transport of the beads primarily to be by kinesin-1. However, kinesin-2 may be playing a role in transport as well. It is possible all three bead types use kinesin-2 for some transport and have different interactions with this motor. It is likely that all three bead types use multiple anterograde motor types at some point during transport. However, because JIP-1 peptide appears to be more efficient than APP-C and negative charge as a cargo motor receptor, it is likely that this JIP-1 peptide has better interactions than APP-C and negative charge with these motor types as well.

Competition between cargo for multiple motors and different microtubules

The above study is also the first to show competition between cargo motor receptors. Through computation analysis, I have shown that at high concentrations of negatively charged beads injected into the axons by Michael Conley and/or Derek Nobrega, the transport machinery saturable. Saturation of kinesin-1 motors had been previously described when individual cargo proteins overexpressed in CAD cells cause mislocalization of endogenous protein (Hammond, et al, 2008). However, this study claims that this mislocalization did not have an effect on localization of other cargo proteins, and thus there is not competition between cargos. I have shown that when JIP-1 peptide beads or APP-C beads were injected into axons with negatively charged beads

(injections performed by Conley and/or Nobrega), JIP-1 peptide beads sustain

movements while inhibiting the movements of negatively charged beads, and that APP-C

beads also sustain movements while inhibiting the movement of negatively charged

beads. It is likely this is a side effect of the high 'on/off' rate of negative charge and the

low 'on/off' rate of JIP-1 peptide and APP-C with the transport machinery, such that JIP-

1 peptide beads and APP-C beads 'steal' motors that have come off negatively charged

particles. Even if this is the case, I have shown that one cargo type, either JIP-1 peptide

beads and/or APP-C beads, can inhibit the transport of another cargo type, negative

charge beads, by 'competing' for, and taking motors. This competition is further

substantiated by the interaction of JIP-1 peptide cargo with APP-C cargo (co-injection of

JIP-1 peptide beads and APP-C beads by Conley/Nobrega). I have shown that both

cargos in this instance initially severely inhibit the others' transport, which is highly

indicative of competition for available motors.

The ability of JIP-1 peptide coated beads to regain transport capabilities, while

still inhibiting APP-C bead transport raises interesting questions of how competition

within the axon for motors might evolve. In this case, JIP-1 peptide beads cannot be not

'taking' more motors from APP-C beads because APP-C bead transport is not further

inhibited even though JIP-1 peptide bead transport frequency is increasing. Thus, JIP-1

peptide beads must be recruiting additional, cryptic, motors. Due to the time course, I

have explained this phenomenon of JIP-1 peptide bead increase in transport by proposing

that JIP-1 peptide beads are recruiting a second, less accessible motor (kinesin-3), as

discussed in the discussion presented in Chapter 2.

Another possible explanation for this phenomenon is that JIP-1 peptide is able to activate inactive kinesin-1 motors and therefore increase its transport frequency. The recent discovery that kinesin-1 is autoinhibited by a single tail region of one of the heavy chains led to experiments showing that cross-linking of the motor domains causes inhibited hydrolysis of ATP (Kaan, et al, 2011). Upon inactivation of kinesin-1, the motor dissociates from the microtubules. An amino acid sequence containing the same amino acids as the JIP-1 peptide used in my analysis is not sufficient to activate kinesin-1 on it's own. However, when this JIP-1 sequence binds kinesin-1 in combination with FEZ1, kinesin-1 can be activated and bind microtubules for motility (Blasius, et al, 2007). It is possible the delayed enhancement of JIP-1 peptide bead movement in the above experiments is due to the time it takes to recruit the endogenous FEZ-1 to kinesin-1 motors for release of the heavy chain tail region of kinesin-1 allowing for ATP hydrolysis and kinesin-1 activation. APP-C bead movements would still not show increased movement from these newly activated motors, because they would still be sequestered on JIP-1 peptide cargo.

This new identification of an inhibitory peptide for the keinsin-1 motor will allow direct testing of the role of the kinesin-1 motor in the squid axon transport system. Since wild-type squid axons are used that cannot be transfected or otherwise genetically altered, this cannot be tested through traditional molecular biology approaches. With a short, injectable peptide, specific inhibition of kinesin-1 is now possible. Thus, using the squid axon as a transport model system, it can be tested to see if 1) JIP-1 peptide, APP-C and negative charge beads use primarily kinesin-1 for transport, and 2) if this JIP-1 peptide can activate kinesin-1 for increased frequency of transport.

Conclusion

I have identified the interactions of three anterograde receptors, JIP-1 peptide, APP-C, and negative charge that display different transport efficiencies. The characterization of the differences in transport behaviors of these cargo motor receptors provides intriguing insight into how a cell might regulate cargo transport through selection of a cargo motor receptor. Negatively charged particles are known to transport in the anterograde direction (Adams and Bray, 1983, and Vale, et al, 1985c), and the surface of cellular organelles are known to be non-uniform and contain negatively charged species (Klopfenstein, et al, 2002). It is possible the cell uses negatively charged species for transport of cargo, but when a cargo is required to reach a destination faster and transport more efficiently, the cell employs a receptor such as JIP-1 peptide or APP-C.

Finally, the protein type selected as the cargo motor receptor may be a transport regulatory mechanism employed by the cell. APP-C is the C-terminal peptide of the transmembrane protein, amyloid precursor protein. As a transmembrane protein, APP is inseparably attached to its cargo throughout transport, while JIP-1 is a soluble scaffolding protein. APP-C has multiple proposed functions outside of being a transport receptor (Zhang, et al, 2011) and JIP-1 has a known other function as a scaffolding protein for the MAPK signaling pathway(s) (Yasuda, et al, 1999). The revelation of JIP-1's active role in transport may be more complex than simply recruiting anterograde transport machinery for more efficient transport. Organelles in a cell have a much less uniform membrane surface than the engineered fluorescent beads in the above experiments. Due

to multiple interacting partners, the soluble nature of JIP-1, and it's role in in signaling pathways, (Yasuda, et al, 1999), JIP-1 may move from cargo to cargo, binding interacting partners on the non-uniform surface of cellular organelles, and either 1) binding retrograde receptors, thereby blocking them from retrograde transport machinery while actively recruiting anterograde machinery, 2) becoming the anterograde motor receptor for an organelle and increasing the efficiency of its transport, and/or 3) transporting signaling complexes concurrently with organelle transport.

The above study has provided important insight into multiple facets of cargo transport. I have explored some of the properties that make for a suitable anterograde cargo motor receptor, and have defined the interactions and competitions between two already known cargo motor receptors, APP-C and negative charge, and a newly identified receptor, JIP-1 peptide. Further studies using the giant axon of the squid will help to further define the spatiotemporal regulatory mechanisms of cargo transport.

Chapter 4: References

Adams RJ & Bray D (1983) Rapid transport of foreign particles microinjected into crab axons. *Nature*303(5919):718-720.

Allen RD, Metuzals J, Tasaki I, Brady ST, & Gilbert SP (1982) Fast axonal transport in squid giant axon. *Science* 218(4577):1127-1129.

Andrews NL, Pfeiffer JR, Martinez AM, Haaland DM, Davis RW, Kawakami T, Oliver JM, Wilson BS, & Lidke DS (2009) Small, mobile FcepsilonRI receptor aggregates are signaling competent. *Immunity* 31(3):469-479.

Barkus RV, Klyachko O, Horiuchi D, Dickson BJ, & Saxton WM (2008) Identification of an axonal kinesin-3 motor for fast anterograde vesicle transport that facilitates retrograde transport of neuropeptides. *Mol Biol Cell* 19(1):274-83.

Bearer EL, DeGiorgis JA, Bodner RA, Kao AW, & Reese TS (1993) Evidence for myosin motors on organelles in squid axoplasm. *Proc Natl Acad Sci U S A* 90(23):11252-11256.

Bearer EL, & Reese TS (1999) Association of actin filaments with axonal microtubule tracts. *J Neurocytol.* 28(2):85-98.

Bearer EL, Breakefield XO, Schuback D, Reese TS, & LaVail JH (2000) Retrograde axonal transport of herpes simplex virus: evidence for a single mechanism and a role for tegument. *Proc Natl Acad Sci U S A* 97(14):8146-8150.

Blasius TL, Cai D, Jih GT, Toret CP, & Verhey KJ (2007) Two binding partners cooperate to activate the molecular motor Kinesin-1. *J Cell Biol* 176(1):11-7.

Brady ST, & Lasek RJ (1982a) Axonal transport: a cell-biological method for studying proteins that associate with the cytoskeleton. *Methods Cell Biol.* 25(Pt B):365-98.

Brady ST, Lasek RJ, & Allen RD (1982b) Fast axonal transport in extruded axoplasm from squid giant axon. *Science* 218(4577):1129-1131.

Brady ST, Pfister KK, & Bloom GS (1990) A monoclonal antibody against kinesin inhibits both anterograde and retrograde fast axonal transport in squid axoplasm. *Proc Natl Acad Sci U S A* 87(3):1061-1065.

Brown A (2003) Axonal transport of membranous and nonmembranous cargoes; a unified perspective. *J Cell Biol.* 160(6): 817-821.

Chou YH, Helfand BT, & Goldman RD (2001) New horizons in cytoskeletal dynamics: transport of intermediate filaments along microtubule tracks. *Curr Opin Cell Biol* 13(1):106-109.

Cole DG, Chinn SW, Wedaman KP, Hall K, Vuong T, & Scholey JM (1993) Novel heterotrimeric kinesin-related protein purified from sea urchin eggs. *Nature* 366(6452):268-70.

Coy DL, Wagenbach M, & Howard J (1999) Kinesin takes one 8-nm step for each ATP that it hydrolyzes. *J Biol Chem* 274(6):3667-71.

DeGiorgis JA, Petukhova TA, Evans TA, & Reese TS (2008) Kinesin-3 is an organelle motor in the squid giant axon. *Traffic* 9(11):1867-1877.

Elluru RG, Bloom GS, & Brady ST (1995) Fast axonal transport of kinesin in the rat visual system: functionality of kinesin heavy chain isoforms. *Mol Biol Cell* 6(1):21-40.

Forman DS, McEwen BS, & Grafstein B (1971) Rapid transport of radioactivity in goldfish optic nerve following injections of labeled glucosamine. *Brain Res* 28(1):119 -130.

Galbraith JA, Reese TS, Schlief ML, & Gallant PE (1999) Slow transport of unpolymerized tubulin an polymerized neurofilament in the squid giant axon. *Proc Natl Acad Sci U S A* 96(20):11589-94.

Gill SR, Schroer TA, Szilak I, Steuer ER, Sheetz MP, & Cleveland DW (1991) Dynactin,

a conserved, ubiquitously expressed component of an activator of vesicle motility mediated by cytoplasmic dynein. *J Cell Biol* 115(6):1639-1650.

Goldstein LS, & Gunawardena S (2000) Flying through the drosophila cytoskeletal genome. *J Cell Biol* 150(2):F63-8.

Grafstein B, & Laureno R (1973) Transport of radioactivity from eye to visual cortex in the mouse. *Exp Neurol* 39(1):44-57.

Grafstein B, & Forman DS (1980) Intracellular transport in neurons. *Physiol Rev.* 60(4);1167-283.

Hall DH, & Hedgecock EM (1991) Kinesin-related unc-104 is required for axonal transport of synaptic vesicles in C. elegans. *Cell* 65(5):837-47.

Hammond JW, Griffin K, Jih GT, Stuckey J, & Verhey KJ (2008) Co-operative versus independent transport of different cargoes by Kinesin-1. *Traffic* 9(5):725-41.

Hammond JW, Huang CF, Kaech S, Jacobson C, Banker G, & Verhey KJ (2010) Posttranslational modifications of tubulin and the polarized transport of kinesin-1 in neurons. *Mol Biol Cell* 21(4):572-583.

Heidemann SR, Landers JM, & Hamborg MA (1981) Polarity orientation of axonal

microtubules. *J Cell Biol* 91(3 Pt 1):661-5.

Hirokawa N, Pfister KK, Yorifuji H, Wagner MC, Brady ST, & Bloom GS (1989)
Submolecular domains of bovine brain kinesin identified by electron microscopy and
monoclonal antibody decoration.   *Cell* 56(5):867-78.

Hirokawa N, & Takemura R (2004) Molecular motors in neuronal development,
intracellular transport and diseases. *Curr Opin Neurobiol* 14(5):564-573.

Hirokawa N, & Takemura R (2005) Molecular motors and mechanisms of directional
transport in neurons. *Nat Rev Neurosci* 6(3):201-214.

Hirokawa N, Noda Y, Tanaka Y, & Niwa S (2009) Kinesin superfamily motor proteins
and Intracellular transport. *Nat Rev Mol Cell Biol* 10(10):682-696.

Hollenbeck PJ (1989) The distribution, abundance and subcellular localization of kinesin.
J Cell Biol. 108(6):2335-42.

Hodgkin AL, Huxley AF, & Katz B (1952a) Measurement of current-voltage relations in
the membrane of the giant axon Loligo. *J Physiol* 116(4):424-448.

Hodgkin AL, & Huxley AF (1952b) Currents carried by sodium and potassium ions
through the membrane of the giant axon of Loligo. *J Physiol* 116(4):449-472.

Hodgkin AL, & Huxley AF (1952c) The componenets of membrane conductance in the giant axon of Loligo. *J Physiol* 116(4):473-496.

Hodgkin AL, & Huxley AF (1952d) The dual effect of membrane potential on sodium conductance in the giant axon of Loligo. *J Physiol* 116(4):497-506.

Holzbaur EL, & Goldman YE (2010) Coordination of molecular motors: from *in vitro* assays to intracellular dynamics. *Curr Opin Cell Biol.* 22(1):4-13.

Horiuchi D, Barkus RV, Pilling AD, Gassman A, & Saxton WM (2005) APLIP1, a kinesin binding JIP-1/JNK scaffold protein, influences the axonal transport of both vesicles and mitochondria in Drosophila. *Curr Biol* 15(23):2137-2141.

Huckaba TM, Gennerich A, Wilhelm JE, Chishti AH, & Vale RD (2011) Kinesin-73 is a processive motor that localizes to Rab5-containing organelles. *J Biol Chem* 286(9):7457 -7467.

Inomata H, Nakamura Y, Hayakawa A, Takata H, Suzuki T, Miyazawa K, & Kitamura N (2003) A scaffold protein JIP-1b enhances amyloid precursor protein phosphorylation by JNK and its association with kinesin light chain 1. *J Biol Chem* 278(25):22946-22955.

Jaffe LA & Terasaki M (2004) Quantitative microinjection of oocytes, eggs, and embryos. *Methods Cell Biol* 74:219-242.

Jung P, & Brown A (2009) Modeling the slowing of neurofilament transport along the mouse sciatic nerve. *Phys Biol* 6(4):046002.

Kaan HY, Hackney DD, & Kozielski F (2011) The structure of kinesin-1 motor-tail complex reveals the mechanism of autoinhibition. *Science* 333(6044):883-5.

Kamal A, Stokin GB, Yang Z, Xia CH, & Goldstein LS (2000) Axonal transport of amyloid precursor protein is mediated by direct binding to the kinesin light chain subunit of kinesin-1. *Neuron* 29(2):449-59.

Kamal A, & Goldstein LS (2002) Principles of cargo attachment to cytoplasmic motor proteins. *Curr Opin Cell Biol* 14(1):63-68.

Kanaan NK, Morfini GA, LaPointe NE, Pigino GF, Patterson KR, Song Y, Andreadis A, Fu Y, Brady ST, & Binder LI (2011) Pathogenic Forms of Tau Inhibit Kinesin Dependent Axonal Transport through a Mechanism Involving Activation of Axonal Phosphotransferases. *J. Neurosc.* 31(27):9895-9904.

Kanai Y, Okada Y, Tanaka Y, Harada A, Terada S, & Hirokawa N (2000) KIF5C, a novel neuronal kinesin enriched in motor neurons. *J Neruosci* 20(17):6374-84.

Karcher RL, Deacon SW, & Gelfand VI (2002) Motor-cargo interactions: the key to transport specificity. *Trends Cell Biol* 12(1):21-27.

Klopfenstein DR, Tomishige M, Stuurman N, & Vale RD (2002) Role of phosphatidylinositol(4,5)bisphosphate organization in membrane transport by the Unc104 kinesin motor. *Cell* 109(3):347-58.

Klopfenstein DR, & Vale RD (2004) The lipid binding pleckstrin homology domain in UNC-104 kinesin is necessary for synaptic vesicle transport in Caenorhabditis elegans. *Mol Biol Cell* 15(8):3729-39.

Kumar J, Yu H, & Sheetz MP (1995) Kinectin, an essential anchor for kinesin-driven vesicle motility. *Science* 267(5205): 1834-7.

Lasek RJ, & Brady ST (1985) Attachment of transported vesicles to microtubules in axoplasm is facilitated by AMP-PNP. *Nature* 316(6029):645-7.

Lasek RJ (1986) Polymer sliding in axons. *J Cell Sci Suppl* 5:161-179.

Matsuda S, Yasukawa T, Homma Y, Ito Y, Kiikura T, Kiraki T, Hirai S, Ohno S, Kita Y, Kawasumi M, Kouyama K, Yamamoto T, Kyriakis JM, & Kishimoto I (2001) c-Jun N terminal kinase (JNK)-interacting protein-1b/islet-brain-1 scaffolds Alzheimer's amyloid

precursor protein with JNK. *J Neurosci* 21(17):6597-6607.

McEwen BS, & Grafstein B (1968) Fast and slow components in axonal transport of protein. *J Cell Biol* 38(3):494-508.

McEwen BS, Forman DS, & Grafstein B (1971) Components of fast and slow axonal transport in the goldfish optic nerve. *J Neurobiol* 2(4):361-377.

Miki H, Okada Y, & Hirokawa N (2005) Analysis of the kinesin superfamily: insights into structure and function. *Trends Cell Biol* 15(9):467-76.

Morfini GA, Burns M, Binder LI, Kanaan NM, LaPointe N, Bosco DA, Brown HR Jr, Brown H, Tiwari A, Edgar J, Nave KA, Garberrn J, Atagi Y, Song Y, Pigino G, & Brady ST (2009) Axonal transport defects in neurodegenartive diseases. *J Neurosci* 29(41):12776-12786.

Muresan V, Stankewich MC, Steffen W, Morrow JS, Holzbaur EL, & Schnapp BJ (1991) Dynactin-dependent, dynein-driven vesicle transport in the absence of membrane proteins: a role for spectrin and acidic phospholipids. *Mol Cell* 7(1):173-183.

Muresan V, Godek CP, Reese TS, & Schnapp BJ (1996) Plus-end motors override minus end motors during transport of squid axon vesicles on microtubules. *J Cell Biol* 135(2):383-397.

Muresan V, Abramson T, Lyass A, Winter D, Porro E, Hong F, Chamerlin NL, & Schnapp BJ (1998) KIF3C and KIF3A form a novel neuronal heteromeric kinesin that associates with membrane vesicles. *Mol Biol Cell* 9(3):637-52.

Muresan V (2000) One axon, many kinesins: What's the logic? *J Neurocytol.* 29(11 12):799-818.

Muresan Z, & Muresan V (2005) Coordinated transport of phosphorylated amyloid-beta precursor protein and c-Jun NH2-terminal kinase-interacting protein-1. *J Cell Biol* 171(4):615-625.

Okada Y, Yamazaki H, Sekine-Aizawa Y, & Hirokawa N (1995) The neuron-specific kinesin superfamily protein KIF1A is a unique monomeric motor for anterograde axonal transport of synaptic vesicle prescursors. *Cell* 81(5):769-80.

Paschal BM, Shpetner HS, & Vallee RB (1987a) MAP 1C is a microtubule-activated ATPase which translocates microtubules in vitro and has dynein-like properties. *J Cell Biol.* 105(3):1273-1282.

Paschal BM, & Vallee RB (1987b) Retrograde transport by the microtubule-associated protein MAP 1C. *Nature* 330(6144):181-183.

Pfister KK, Wagner MC, Stenoien DL, Brady ST, & Bloom GS (1989) Monoclonal antibodies to kinesin heavy and light chains stain vesicle-like structures, but not microtubules, in cultured cells. *J Cell Biol.* 108(4):1453-63.

Prahlad V, Helfand BT, Langford GM, Vale RD, & Goldman RD (2000) Fast transport of neurofilament protein along microtubules in squid axoplasm. *J Cell Sci* 113(Pt 22):3939-3946.

Rahman A, Friedman DS, & Goldstein LS (1998) Two kinesin light chain genes in mice. Identification and characterization of the encoded proteins. *J Biol Chem* 273(25):15395 -403.

Satpute-Krishnan P, DeGiorgis JA, & Bearer EL (2003) Fast anterograde transport of herpes simplex virus: role for the amyloid precursor protein of alzheimer's disease. *Aging Cell* 2(6):305-318.

Satpute-Krishnan P, DeGiorgis JA, Conley MP, Jang M, & Bearer EL (2006) A peptide zipcode sufficient for anterograde transport within amyloid precursor protein. *Proc Natl Acad Sci U S A* 103(44):16532-16537.

Sau D, Rusmini P, Crippa V, Onesto E, Bolzoni E, Ratti A, & Poletti A (2011) Dysregulation of axonal transport and motorneuron diseases. *Biol Cell* 103(2):87-107.

Schnapp BJ, Vale RD, Sheetz MP, & Reese TS (1985) Single microtubules from squid axoplasm support bidirectional movement of organelles. *Cell* 40(2):455-462.

Schnapp BJ, & Reese TS (1989) Dynein is the motor for retrograde axonal transport of organelles. *Proc Natl Acad Sci U S A* 86(5):1548-52.

Schnapp BJ, Reese TS, & Bechtold R (1992) Kinesin is bound with high affinity to squid axon organelles that move to the plus-end of microtubules. *J Cell Biol.* 119(2):389-399.

Schroer TA, Steuer ER, & Sheetz MP (1989) Cytoplasmic dynein is a minus end-directed motor for membranous organelles. *Cell* 56(6):937-46.

Schroer TA, & Sheetz MP (1991) Two activators of microtubule-based vesicle transport. *J Cell Biol* 115(5):1309-1318.

Sheetz MP (1996) Microtubule motor complexes moving membranous organelles. *Cell Struct Funct* 21(5):369-73.

Stenoien DL, & Brady ST (1997) Immunochemical analysis of kinesin light chain function. *Mol Biol Cell* 8(4): 675-89.

Svoboda K, Schmidt CF, Schnapp BJ, & Block SM (1993) Direct observation of kinesin stepping by optical trapping interferometry. *Nature* 365(6448):721-7.

Taru H, Iijima K, Hase M, Kirino Y, Yagi Y, & Suzuki T (2002) Interaction of Alzheimer's beta -amyloid precursor family proteins with scaffold proteins of the JNK signaling cascade. *J Biol Chem* 277(22):20070-20078.

Terada S, Kinjo M, & Hirokawa N (2000) Oligomeric tubulin in large transporting complex is transported via kinesin in squid giant axons. *Cell* 103(1):141-55.

Terasaki M, Schmidek A, Galbraith JA, Gallant PE, & Reese TS (1995) Transport of cytoskeletal elements in the squid giant axon. *Proc Natl Acad Sci U S A* 92(25):11500 -11503.

Toyoshima I, Yu H, Steuer ER, & Sheetz MP (1992) Kinectin, a major kinesin-binding protein on ER. *J Cell Biol.* 118(5):1121-31.

Vale RD, Reese TS, & Sheetz MP (1985a) Identification of a novel force-generating protein, kinesin, involved in microtubule-based motility. *Cell* 42(1):39-50.

Vale RD, Schnapp BJ, Reese TS, & Sheetz MP (1985b) Movement of organelles along filaments dissociated from the axoplasm of the squid giant axon. *Cell* 40(2):449-454.

Vale RD, Schnapp BJ, Reese TS, & Sheetz MP (1985c) Organelle, bead, and microtubule translocations promoted by soluble factors from the squid giant axon. *Cell*40(3):559-569.

Vale RD, Schnapp BJ, Mitchison T, Steuer E, Reese TS, & Sheetz MP (1985d) Different axoplasmic proteins generate movement in opposite directions along microtubules *in vitro*. *Cell* 43((3 Pt 2)):623-632.

Vale RD, & Fletterick RJ (1997) The design plan of kinesin motors. *Annu Rev Cell Dev Biol* 13:747-77.

Verhey KJ, Meyer D, Deehan R, Blenis J, Schnapp BJ, Rapoport TA, & Margolis B (2001) Cargo of kinesin identified as JIP scaffolding proteins and associated signaling molecules. *J Cell Biol* 152(5):959-970.

Yang JT, Laymon RA, & Goldstein LS (1989) A three-domain structure of kinesin heavy chain revealed by DNA sequence and microtubule binding analyses. *Cell* 56(5):879-89.

Yang JT, Saxton WM, Stewart RJ, Raff EC, & Goldstein LS (1990) Evidence that the head of kinesin is sufficient for force generation and motility *in vitro*. *Science* 249(4964):42-7.

Yasuda J, Whitmarsh AJ, Cavanagh J, Sharma M, & Davis RJ (1999) The JIP group of mitogen activated protein kinase scaffold proteins. *Mol Cell Biol* 19(10):7245-7254.

Yildiz A, Tomishige M, Vale RD, & Selvin PR (2004) Kinesin walks hand-over-hand. *Science* 303(5658):676-678.

Yildiz A, Tomishige M, Gennerich A, & Vale RD (2008) Intramolecular strain coordinates kinesin stepping behavior along microtubules. *Cell* 134(6):1030-1041.

Yuan A, Kumar A, Peterhoff C, Duff K, Nixon RA (2008) Axonal transport rates in vivo are unaffected by tau deletion or overexpression in mice. *J Neurosci* 28(7):1682-1687.

Zhang YW, Thompson R, Zhang H, & Xu H (2011) APP processing in Alzheimer's disease. *Mol Brain* 7(4):3-10.

Appendix I: Protocols

Measuring Bead Moves in Squid Axon Videos Using Metamorph

Exporting Videos and Aligning Frames

1. Open LSM Image Browser.

2. Open .mdb file for appropriate .lsm format video.

3. Scroll through .mdb until you find the .lsm format video. Double click to open.

4. Once the video is open, you can add a magnification bar by clicking on the appropriate icon to the right. You can also add this later in Metamorph. See below.

5. To add a time stamp, click on the "A" icon to the right. A box will open. Click "time". Choose appropriate units.

6. To export the video, click export.

7. Make sure the parameters for export are "contents of window series", "no compression", and a simple .tif sequence format.

8. Save using appropriate name.

9. Open Metamorph.

10. Go to "File", then select "Open Special", then select "Build Stack". Choose exported .tif sequence.

11. In the menu, go to "Stack" and select "Keep Planes…" Select desired planes and select *Apply*.
12. From the "Stack" Menu, select "Align Stack…" The Align Stack dialog box will appear.
13. From the *Display* group, select *Subtract.* This uses subtraction to show the difference between the reference plane and the shifting plane.
14. Specify the location of the reference plane for the alignment using *Reference* as *Adjacent (n-1)*. This will set the reference plane to the plane Adjacent to the current plane.
15. Use the *Horizontal Shift* and *Vertical Shift* text boxes or sliders to adjust the alignment of the plane displayed in the alignment image window. The plane will be moved in one-pixel increments.
16. The plane will be aligned when there is a nearly uniform grayscale level throughout the entire image.
17. Be sure to select *Auto Next* and choose *Apply* when you are satisfied with the alignment of the plane. This will advance the stack to the next plane.
18. Repeat Steps 5-7 until you have aligned each plane in the stack.

19. Save as either .stk or .tif image sequence.

Measuring Bead Moves

1. If not previously done, from the "Measure" menu, choose calibrate. Make sure the calibration in Metamorph matches that of the mdb for the video in question.

2. From the Display menu, choose "Graphics", choose "Calibration Bar".

3. From the "Apps" menu, choose "Track Points…" The Track Points dialog box opens.

4. Select the image source from the *Source* radio button group as *Stack*.

5. Select "Set Interval…" from the Track Points dialog box. Make sure the Table Time Units are in seconds, and the Time Interval Options is set to "Time of Image Creation".

6. Select "Set Overlay" from the Track Points dialog box. Make sure that "Display Track Path" is selected and "Display Track Pattern" is deselected.

7. Select "Add Track" from the Track Points dialog box, and using your pointer, click the bead in the first image that you want to track. The next plane will be displayed automatically. Make sure that you are zoomed in on the stack so that you can accurately click on the bead.

8. To advance to the next frame without recording a measurement (i.e. when the bead does not move for one or more frames), press the "+" button on the keyboard. (Similarly, to go back a frame, press the "-" button on the keyboard.

9. Add the next point in this plane, and repeat for all planes in the stack. Your points will be indicated by an image window overlay, and the data associated with the points will be displayed horizontally in the Track Points table. Additional tracks can be defined, as needed.

10. To save the Track Points data, open a data log by choosing *Open Log*. The Open Data Log dialog box opens. Select "Dynamic Data Exchange (DDE)" and press *OK*. The Export Log Data dialog box opens. Select Microsoft Excel as the Application. You can now log your data by choosing the Log Data command in the Track Points dialog box. To view your data, choose View Current Data Log from the Log menu.

Generating Stack Arithmetic and Kymographs

Stack Arithmetic
1. Open ImageJ. Click on the menu "File". Choose "Open>Image Sequence". Choose desired aligned .stk or .tif sequence.
2. Using the mouse, draw a box around an area of particles you wish to 'crop'. Try to select a region as far out on the plume so that as many individual beads as possible can be measured.
3. Save cropped image as a .tif image sequence so that is can be opened in Metamorph.
4. Open Metamorph. Select "File>Open Special>Build Stack". Select the cropped video.
5. Select "Display>Color Separate".
6. Choose the red or green channel. Go to "Process>Stack Arithmetic". In the box that opens, be sure to select "Maximum". Hit "Apply".
7. Save resulting image as a .tif file.

Kymographs
1. Open Metamorph. Select "File>Open Special>Build Stack". Select the cropped video.
2. Select "Display>Color Separate". Program will not do kymographs of merged colors.
3. Select "Stack>Kymograph". Select appropriate source stack from the pop-up box (red, green).
4. Make sure all planes of the video are selected so the kymograph is of the entire video.
5. Select the line width to determine the pixel width/area that will be measured to generate the kymograph.
6. Use the line tool in Metamorph to draw a line across the entire video over the top, middle, and bottom of the plume of particles.
7. Click "Create".
8. Go to "Display>Graphics>Calibration Bar". (Proper mag bars should be generated, as the video used to generate the kymographs should have already been calibrated using the mdb file.)

9. Save as .tif file.

Organizing Spreadsheets Generated from Metamorph and Measuring Behaviors

1. After logging data of tracked particles from Metamorph (see above), save as appropriately labeled Excel file.

2. The spreadsheet generated will give many measurements, such as Image Plane, Elapsed Time, X, Y, Z, Distance, Time Interval, Distance to Origin, Velocity, Delta X, Delta Y, and Pause Duration.' This spreadsheet will also label particles as 1, 2, 3, etc.

3. Make a row with the above measurements labeled, one in each column, labeled in bold.

4. Determine where the particle measurements for a new particle begin (i.e. the label changes from 1 to 2, 2 to 3, etc.).

5. Insert a blank row of cells in between these particles.

6. Copy and past the labels into these blank cells for the new particle.

For Each Particle

1. To determine the average instantaneous velocity, average the column containing the behavior "velocity". For example "=AVERAGE(I4:I63). (This will not include pauses.)

2. Using the appropriate statistical analysis in Excel, determine the standard deviation of the average instantaneous velocity. For example, = STDEV(I4:I63).

3. To determine the average velocity, divide the farthest "Distance to Origin" measurement for each individual particle by the sum of the "Time Interval" column. (This will include pauses and will give the average rather than instantaneous).

4. To determine the maximum velocity, command Excel "=MAX for the column containing velocity". For example "=MAX(I4:I63)".

5. To determine the run duration of a particle, add (sum) the "Time Interval" column.

6. To determine the number of pauses, count how many times there is a number OTHER THAN 0 in the "Pause Duration" column. A 0 indicates there is no pause.

7. To determine the "Pause Duration" of a particle, add (sum) the column containing the "Pause Duration".

8. To determine the percentage of time paused, divide the Pause Duration just measured by the Run Duration previously measured.

Combining Particle Behaviors

1. To determine the Total Average Instantaneous velocity of all particles of one bead type, average all measurements of instantaneous velocity.

2. Apply the standard deviation function in Excel to determine the standard deviation of this average.

3. To determine the Maximum velocity displayed across ALL particles, use "=MAX (Column:Column)". For example, "=MAX(I:I).

4. To determine the number of moves, count the column with the number of measured velocities. For example, "=COUNT (I4:I63, I66:I108, etc.)".
5. To determine the Average Instantaneous Velocity for Each Bead Path, average the measurements of average instantaneous velocity for each particle. For example, "=AVERAGE(N4, N68, etc.)."
6. To determine the standard deviation for the average instantaneous velocity for each bead path, use the standard deviation function in Excel for the previous calculation.
7. To determine the Number of Beads, count the number of beads measured.
8. To determine the Total Duration Time, add (sum) the Run Duration measured for each particle. For example, "=SUM(N19, N81, etc.)".
9. To determine the Total Pause Time, add (sum) the Pause Duration Measured for each particle. For example, "=SUM(N25, N87, etc.)".
10. To determine the Total Time Moving, Subtract the Total Pause Time from the Total Duration Time.
11. To determine the % Total Time Moving, divide the Total Time Moving by the Total Duration Time.
12. To determine the % Total Time Paused, divide the Total Pause Time by the Total Duration Time.
13. To determine the Average Run Duration, divide The Total Duration Time by the number of particles measured.
14. To determine the standard deviation for the Average Run Duration, use the standard deviation function in Excel.
15. To determine the Total Run Length, add (sum) the longest "Distance to Origin" for each particle.
16. To determine the Average Run Length, divide the Total Run Length by the number of particles.
17. To determine the standard deviation for Average Run Length, use the standard deviation function in Excel.

Organizing Spreadsheets for CPA and Kolmogrov-Smirnov Statistics

Organizing Spreadsheets
1. Copy the organized spreadsheets from Metamorph into a new Excel file.
2. In the new Excel file, remove the breaks that separated each particle.
3. Copy the columns that contain the behaviors "Distance", "Time Interval", and "Velocity".
4. Remove all "0"s from the "Pause Duration", and copy over to the new spreadsheet.
5. Create a new column labeled "Run Lengths".
6. To determine individual run lengths before pauses of a particle, look at the copied organized spreadsheet from Metamorph. Look at the "Pause Duration" column. For each "0" add the "Distance" in that row to the "Distance" listed in the above row. Do this until you encounter a number in the "Pause Duration" column OTHER THAN "0". A number other than "0" indicates a pause. Repeat until all run lengths are calculated.
7. To determine the Run Duration of each Run Length, add the number of "0's" and the first "number other than "0" encountered from the Pause Duration column of the original spreadsheet.
8. To determine the Run Velocity of each run, divide the Run Length by the Run Duration.
9. To determine the Total Time, add (sum) the "Time Interval" column.
10. To determine the Total Time Paused, add (sum) the edited "Pause Duration" column.
11. To determine the Average Run Velocity, average the column containing the calculated run velocities.
12. To determine the standard deviation for the Average Run Velocity, use the standard deviation function in Excel.
13. Multiple axon injection conditions analyzed in this way can be combined into one spreadsheet, making sure to differentiate them as the different conditions. Combining into one spreadsheet will be important for uploading data into MATLAB for analysis.
14. Once analysis is done and spreadsheets are made, save as "JIP-1, APP-C, or Negative Charge Combined Velocities". Alternatively, save them as "JIP-1, APP-C, or Negative Charge Processed Axons".

Using MATLAB for CPA Analysis and Kolmogorov-Smirnov Statistics

Thank you to Pat Cutler for his help in writing the MATLAB Scripts for this Analysis

1. The above, prepared spreadsheets have already been imported into MATLAB. They are labeled JIP-1_APP-C_and_Negative_Charge_Data_for_CPA_Analysis.mat.
2. Open MATLAB, and drag and drop this file into the command window.
3. Make sure all files you will be working with (Scripts, Data, etc.) to do this analysis are in ONE folder, and that this folder is addressed as the "Current Directory" in MATLAB.
4. The way the data has been imported, only conditions of JIP-1, APP-C, and Negative Charge when co-injected with glycine will be analyzed and compared. (Having all conditions on one spreadsheet makes importing all of the data and re-writing code to compare all conditions at a later time easier).
5. To determine what behaviors can be compared, type data.rawData in the command window. This will bring up the commands you will want to use to change what you are analyzing/comparing. For example, it will bring up labels such as runVelocity, runLength, pauseDuration, etc.
6. Open the script labeled "multCPA.m".
7. Open the script labeled CPA_Analysis.m. Look to see what behavior is being compared. You can change this by typing "control F", finding a behavior, and "replacing all" with another behavior. For example, if you want to compare runLengths but the script is currently comparing runDurations, click "control F" and "replace all" runDurations with runLengths.
8. Hi-light this script and hit F9. This will generate a CPA plot from the data. You can use the arrow at the top of the MATLAB program to open the graph editor, and makes changes to the plot that has been generated.
9. Open the script labeled KSTest.m. Make sure that the script for this is comparing the same behavior as the CPA_Analysis.m script. For example, make sure both are comparing runLengths.
10. Hi-light this script and hit F9. This will give you statistical P values and KS values of the behaviors you are comparing. For example, this will give you statistics comparing runLengths of JIP-1 with Glycine vs. Negative Charge with Glycine vs. APP-C with glycine.

Counting Percent Beads Moving

1. Open the folder containing the aligned 100 .tif file sequence of a video.
2. Make ten folders, labeled for the video, frames 1-10, 11-20, etc.
3. Copy and paste the first ten .tif files into the folder labeled 1-10. Copy and pasted .tif files 11-20 into the folder labeled 11-20, etc.
4. Open Metamorph. Go to "File>Open Special>Build Stack". Open the appropriate folder containing the smaller sequence of .tif files (Folder labeled 1-10, etc.).
5. In the first frame of all sets of sequences, count as many individual beads as you can. Write this number down.
6. Go to "Process>Stack Arithmetic". In the box that opens, be sure to select "Maximum". Hit "Apply".
7. Count the number of STREAKS you see. These are MOVING beads. Write this number down.
8. To determine the percentage of beads moving in each ten frame increment, divide the number of streaks counted by the total number of beads counted, and multiply by 100.
9. Use Excel to make a graph of percentage of beads moving in each ten frame increment over a 100 frame video.